

Modeling of Plasticity-Induced Crack Closure Under Creep-Fatigue Variable Amplitude Loading

A Thesis

Presented in the Partial Fulfillment of the Requirements for the

Degree of Master of Science

with a

Major in Mechanical Engineering

in the

College of Graduate Studies

University of Idaho

by

Srijan Bhandari

Major Professor: Gabriel Potirniche, Ph.D.

Committee Members: Robert Stephens, Ph.D.; Michael Maughan, Ph.D.

Department Chair: Gabriel Potirniche, Ph.D.

May 2023

ABSTRACT

Finite element simulations of fatigue crack growth (FCG) and creep-fatigue crack growth (CFCG) under constant amplitude (CA) and variable amplitude (VA) loading waveforms are performed to investigate the mechanics of crack opening and closing, which has implications on crack growth rate. The material of study is the ferritic-martensitic steel 9Cr-1Mo (modified 9Cr-1Mo) at 625 °C. Two-dimensional finite element analyses of compact tension (CT) specimens are performed to simulate crack growth under several VA loading scenarios, considering elastic-plastic and creep deformation of the material at the crack tip. In this study, the relevant variable influencing crack growth rate is the crack opening load, caused by the phenomenon of plasticity-induced crack closure. A series of loading conditions were simulated using the finite element method, i.e., fatigue overload (OL) in either CA FCG or CFCG waveforms, creep-fatigue OL in CFCG waveforms, and underload (UL) in CFCG waveforms. The crack opening loads obtained from this study for CA loading in both FCG and CFCG, agree with data from published studies. This study found that a significant reduction in crack opening loads is experienced by the growing crack when an OL or UL cycle was introduced. Immediately after the OL or UL cycle is applied, the crack opening load increases during both fatigue OL and creep-fatigue OL to values larger than those recorded during CA FCG and CFCG loading, whereas UL waveforms resulted in consistently lower crack opening loads. The increase in crack opening loads is proportional to both the extent of OL and the duration of hold time in the OL cycle. However, following the application of a UL, the crack opening loads in the subsequent cycles were not influenced by the magnitude of the UL or the duration of hold time in the UL cycle.

KEYWORDS: plasticity-induced crack closure, opening load, variable amplitude loading, crack growth, creep-fatigue

ACKNOWLEDGEMENTS

I would like to express my deepest appreciation to my major professor, Dr. Gabriel Potirniche, for his invaluable guidance and support throughout my research. His expertise, knowledge, and willingness to help have been instrumental in shaping my work and making it possible to reach this point. Without his continuous encouragement and invaluable advice, this work would not have been possible. I would also like to thank the members of my thesis committee, Dr. Robert Stephens, and Dr. Michael Maughan, for their support during my master's program at the University of Idaho.

I would also like to acknowledge Jose Ramirez, a previous graduate student at the University of Idaho, who assisted me during the research process. Thank you for giving me time out of your busy schedule, sharing your knowledge, and helping me with the setup and data analysis. Additionally, I am grateful for the scholarships from the Department of Mechanical Engineering, the University of Idaho, and the Hayes family. Their financial support provided me with the necessary resources and helped me focus on my research. Thank you for believing in me and supporting my academic pursuit.

DEDICATION

This thesis is dedicated to my family, who have been my unwavering support, encouragement, and source of love throughout my academic journey. Their belief in me has been a constant source of motivation, pushing me to strive for excellence and never give up on my dreams. I am forever grateful for their sacrifices and encouragement, which have made it possible for me to pursue my academic goals.

I would also like to express my heartfelt gratitude to my wife for her unwavering support, love, and patience. She has been my rock throughout this journey, always believing in me and pushing me to be my best. Her support has been immeasurable, and I could not have done this without her by my side.

To my family and my wife, thank you for always being there for me, for understanding my busy schedule, and for supporting me in every way possible. Thank you all for being a part of my journey and helping me achieve this significant milestone.

TABLE OF CONTENTS

ABSTRACT.....	ii
ACKNOWLEDGEMENTS.....	iii
DEDICATION.....	iv
TABLE OF CONTENTS.....	v
LIST OF FIGURES.....	vii
LIST OF TABLES.....	ix
NOMENCLATURE.....	x
CHAPTER 1: INTRODUCTION.....	1
CHAPTER 2: LITERATURE REVIEW.....	2
2.1 Loading modes and crack growth.....	2
2.2 Crack closure.....	4
2.3 Constant amplitude loading on FCG and CFCG.....	5
2.4 Variable amplitude loading on FCG and CFCG.....	6
CHAPTER 3: FINITE ELEMENT MODELING.....	8
3.1 Specimen geometry and material modeling.....	8
3.2 Meshing and boundary conditions.....	9
3.3 Loading waveforms and crack growth scheme.....	11
CHAPTER 4: MODEL VALIDATION.....	14
CHAPTER 5: RESULTS AND DISCUSSION.....	17
5.1 Constant amplitude loading during CA FCG and CFCG.....	17
5.2 Single overload cycle during FCG.....	21
5.3 Variable amplitude loading during CFCG.....	23

5.3.1 Single creep-fatigue OL.....	23
5.3.2 Single fatigue OL.....	29
5.4 Single creep-fatigue UL	33
CHAPTER 6: CONCLUSIONS AND FUTURE WORK.....	35
REFERENCES	36
APPENDIX.....	40

LIST OF FIGURES

Figure 1. Three modes of crack extension.....	2
Figure 2. Representation of opening and effective stress intensity factors.....	5
Figure 3. Geometry of the CT specimen used in the finite element simulations.....	8
Figure 4. Partitioning of two-dimensional CT specimen.....	10
Figure 5. Finite element mesh and boundary conditions for the two-dimensional CT specimen. (a) full specimen mesh, (b) close-up of the most refined region.	11
Figure 6. Loading waveforms for (a) Fatigue overload in a FCG cycle, (b) Creep-fatigue overload in a CFCG cycle, (c) Fatigue overload in a CFCG cycle, and (d) Creep-fatigue underload in a CFCG cycle.....	13
Figure 7. Opening load comparison between the present and previously published data during constant amplitude FCG	14
Figure 8. Predictions of normalized opening loads during constant amplitude FCG for different load ratios.	15
Figure 9. Variation of crack-tip opening loads with ΔK during CA CFCG with different hold times.....	16
Figure 10. Normalized crack opening loads during constant amplitude FCG and CFCG for $t_H = 60$ s and $t_H = 600$ s.	17
Figure 11. (a) Contact stresses behind the crack tip at minimum load in cycle 41, and (b) equivalent von Mises stresses ahead of the crack tip at maximum load in cycle 41 after hold time.	19
Figure 12. Crack-tip region during CA CFCG with hold times in cycle 41 in (a) $t_H = 60$ s, (b) $t_H = 600$ s, (c) $t_H = 60$ s, and (d) $t_H = 600$ s. Contour plots of equivalent plastic strains (PEEQ) in (a) and (b), equivalent creep strains (CEEQ) in (c) and (d).....	20
Figure 13. Single overload effect on crack-tip opening loads during CA FCG.	22
Figure 14. Contour plots of equivalent plastic strains in cycle 41 in (a) CA FCG and (b) OLR = 1.15 in FCG, and in cycle 58 in (c) CA FCG and (d) OLR = 1.15 in FCG.....	23
Figure 15. Effects of single creep-fatigue overload on crack opening loads during CFCG... ..	24

Figure 16. Effects of single creep-fatigue overload in cycle 69 (between node releases 34 and 35) on the (a) crack opening displacement and (b) contact stresses, behind the crack tip crack-tip..	26
Figure 17. Contour plots of equivalent plastic strains in cycle 69 after hold time during (a) constant amplitude CFCG, $t_H = 60$ s, (b) OLR = 1.15 and $t_{OH} = 3600$ s in CFCG with $t_H = 60$ s (c) constant amplitude CFCG, $t_H = 600$ s, and (d) OLR = 1.15 and $t_{OH} = 3600$ s in CFCG with $t_H = 600$ s.....	27
Figure 18. Contour plots of equivalent creep strains in cycle 69 after hold time (a) constant amplitude CFCG, $t_H = 60$ s, (b) OLR = 1.15 and $t_{OH} = 3600$ s in CFCG with $t_H = 60$ s (c) constant amplitude CFCG, $t_H = 600$ s, and (d) OLR = 1.15 and $t_{OH} = 3600$ s in CFCG with $t_H = 600$ s.....	29
Figure 19. Effects of single fatigue overload on (a) crack opening loads during CFCG with hold times 60 s and 600 s (b) crack opening displacements in cycle 69 after hold time.....	31
Figure 20. Crack-tip region during CFCG with $t_H = 60$ s in cycle 69 after hold time. Contour plots of equivalent plastic strains for (a) constant amplitude loading and (b) fatigue OL with OLR = 2. Contour plots of equivalent creep strains for (c) constant amplitude loading and (d) fatigue OL with OLR = 2.....	33
Figure 21. Effects of underload ratio and hold time on crack opening load in CFCG.	34

LIST OF TABLES

Table 1. Dimensions for the CT specimen.....	9
Table 2. Mechanical properties of modified 9Cr-1Mo.	9

NOMENCLATURE

a	Crack length
B	Thickness of a compact-tension specimen
W	Width of a compact-tension specimen
P_{max}	Maximum load in a fatigue cycle
P_{min}	Minimum load in a fatigue cycle
R	Fatigue stress/load ratio, $\frac{P_{min}}{P_{max}}$
P_{OP}	Crack-tip opening load
$\frac{P_{OP}}{P_{max}}$	Normalized crack opening load
K_{max}	Maximum stress intensity
K_{min}	Minimum stress intensity
L_T	Loading time
ΔK	Stress intensity range ($K_{max} - K_{min}$)
K_{OP}	Stress intensity factor required to fully open the crack
ΔK_{eff}	Effective stress intensity range ($K_{max} - K_{OP}$)
P_{OL}	Overload during crack growth
P_{UL}	Underload during crack growth
t_H	Load hold at maximum load during constant amplitude FCG and CFCG
t_{OH}	Load hold at maximum load during the OL cycle
t_{UH}	Load hold time at minimum underload during UL cycle
U_T	Unloading time

LIST OF ACRONYMS

CA Constant amplitude loading

CEEQ Equivalent (von Mises) creep strain

CFCG Creep-fatigue crack growth

COD Crack opening displacement

CT Compact-tension specimen

FCG Fatigue crack growth

FEM Finite element method

OL Overload

PEEQ Equivalent (von Mises) plastic strain

UL Underload

OLR Overload ratio

ULR Underload ratio

SYM Strip-yield modeling

VA Variable amplitude loading

CHAPTER 1: INTRODUCTION

Structural components used in power generation and aerospace industries, such as steam headers, steam turbines, gas turbines, and nuclear reactor components, require high fracture strength and toughness at elevated temperatures. These components typically operate under a sequence of variable amplitude (VA) cyclic and steady loads with high temperature exposure [1-3]. Thus, crack formation and propagation lead to failure resulting from the combination of creep and fatigue VA loads during in-service conditions. The synergistic interactions between creep and plastic deformations during creep-fatigue crack growth (CFCG) are complex, particularly in the case of growing cracks. The constant amplitude (CA) fatigue crack growth (FCG) and CFCG have been extensively studied by researchers through experiments and numerical analyses. Also, both experimental and numerical studies have been conducted to study the influence of VA FCG, however, there has been a lack of systematic computational studies on CFCG under VA loading scenarios. The purpose of this study is to investigate how different VA loading scenarios influence the mechanics of crack opening and closing by determining the crack opening loads using the finite element method (FEM). A compact-tension (CT) specimen was used in this study and modified 9Cr-1Mo (ferritic-martensitic steel) at 625 °C was the material of choice. Modified 9Cr-1Mo steel is a ferritic-martensitic steel with high strength, corrosion resistance, and high creep resistance at high temperatures, making it a potential candidate material for high-temperature and high-pressure applications. The results of this study can be extrapolated in a qualitative sense to other engineering materials used at elevated temperatures.

CHAPTER 2: LITERATURE REVIEW

2.1 Loading modes and crack growth

The existence of a crack or other irregularity in a component can cause a significant reduction in its strength. Even if the initial size of the crack or discontinuity is not large enough to cause an immediate failure, subcritical crack growth may occur over time. This means that the crack or discontinuity may gradually increase in size until it reaches a critical point, at which point the component may fail catastrophically. There are three distinct modes of loading by which a crack in structural components can extend, as shown in Figure 1 [4]. Mode I refers to a situation where the applied load causes the crack to open perpendicular to its plane, and it is a prevalent type of failure in structural components. The present study focuses on this specific type of loading. On the other hand, Mode II involves a sliding force parallel to the crack plane, while Mode III is related to a tearing force that acts parallel to the crack plane. When two different modes of loading act together, it is referred to as mixed-mode loading.

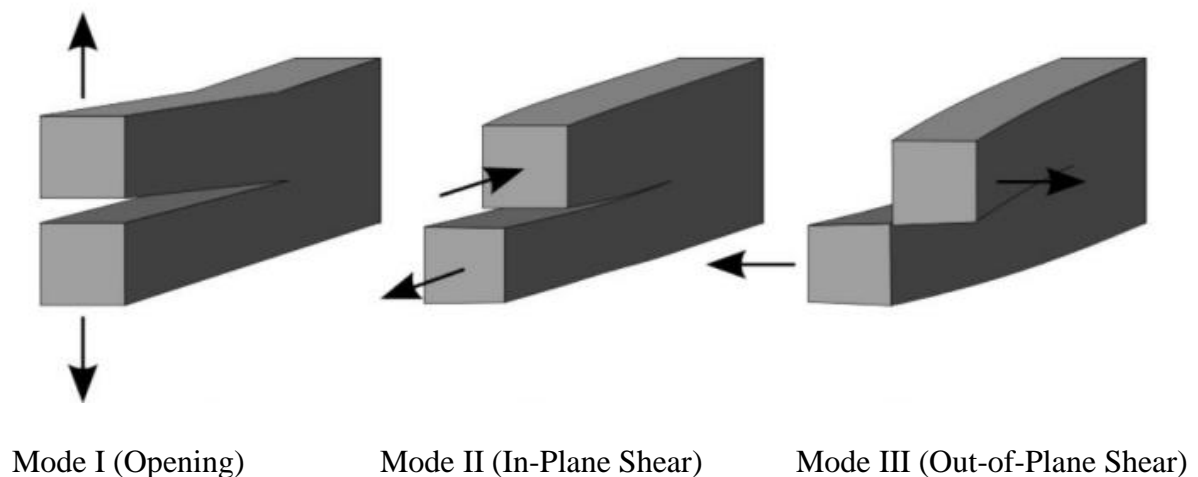


Figure 1. Three modes of crack extension [4].

In structural components subjected to such loading conditions, the stress intensity factor, K , is used to quantify the crack tip driving force. The general equation of K for Mode I loading is shown in equation 1

$$K = S\sqrt{\pi a}F\left(\frac{a}{W}\right) \quad (1)$$

From ASTM E2760: Standard Test Method for Measurement of Fatigue Crack Growth Rates [5], for a CT specimen geometry used in this study, the stress intensity factor K is computed by equation 2.

$$K = \frac{P}{B\sqrt{W}}F\left(\frac{a}{W}\right), \quad (2)$$

$F\left(\frac{a}{W}\right)$ is a geometrical factor, given by equation 3

$$F\left(\frac{a}{W}\right) = \left[\frac{2 + \frac{a}{W}}{\left(1 - \frac{a}{W}\right)^{3/2}} \right] \left(0.886 + 4.64 \left(\frac{a}{W}\right) - 13.32 \left(\frac{a}{W}\right)^2 + 14.72 \left(\frac{a}{W}\right)^3 - 5.6 \left(\frac{a}{W}\right)^4 \right). \quad (3)$$

where a is the crack length, W is the specimen width, B is the thickness of the specimen without a side groove, and P is the applied load.

The geometry of a specimen is an important factor to consider when evaluating the fracture toughness and mechanical properties of a material. The general consideration is that the thin specimen will experience plane stress, while an increase in the thickness will lead to a plane strain condition. The fracture toughness of a material is also affected by various factors such as material properties, strain rate, temperature, and crack length in the specimen.

During a CA cyclic fatigue loading, the rate of crack growth is given by the Paris-Erdogan power law [6],

$$\frac{da}{dN} = A(\Delta K)^n \quad (4)$$

where da/dN represents the FCG rate, A and n are the material constant, and ΔK is the nominal stress intensity factor range. The stress intensity factor range is defined as

$$\Delta K = K_{max} - K_{min} \quad (5)$$

where K_{max} is the maximum stress intensity and K_{min} is the minimum stress intensity during a fatigue cycle.

2.2 Crack closure

Elber [7] experimented on thin sheets of 2024-T3 aluminum alloy to quantify the crack closure concept. Figure 2 shows the concept of effective stress intensity factor range, ΔK_{eff} , which replaced ΔK in equation (4) and can explain the behavior of crack growth in materials during cyclic loading at various load ratios. ΔK_{eff} is defined as

$$\Delta K_{eff} = K_{max} - K_{OP} \quad (6)$$

where K_{OP} is the stress intensity factor required to fully open the crack. The opening stress intensity factor, K_{OP} , is greater than K_{min} . In the portion of loading cycle below K_{OP} , the crack is closed, therefore, the applied load has no effect on FCG. The effective crack tip

driving force, ΔK_{eff} , is less than ΔK due to the plastic deformation behind the crack tip. Rearranging the ΔK_{eff} equation (6) gives,

$$\Delta K_{eff} = K_{max} - K_{OP} = K_{max} \left(1 - \frac{K_{OP}}{K_{max}} \right) \quad (7)$$

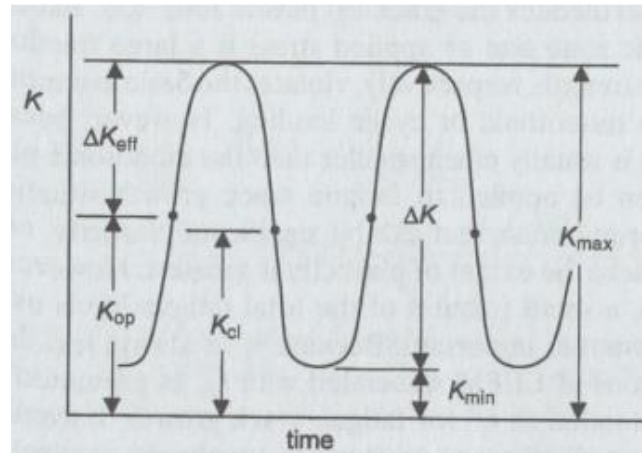


Figure 2. Representation of opening and effective stress intensity factors [4].

The load ratio, R , is the ratio of the minimum load to the maximum load, P_{min}/P_{max} . At a high-load ratios ($R > 0.5$), crack closure is limited, while at a low-load ratios ($R < 0.5$) there is more significant crack closure during crack growth. From equations (2) and (7), it can be observed that $K_{OP}/K_{max} = P_{OP}/P_{max}$.

2.3 Constant amplitude loading on FCG and CFCG

Understanding how the material behaves under stress is crucial, and the study of crack growth plays an important role in this regard. Numerous experimental and numerical studies have been performed to characterize the FCG and CFCG behavior under constant amplitude (CA) loading in structural metals at high temperatures [8-17]. Triangular or trapezoidal loading waveforms have been commonly used to simulate the FCG and CFCG in these studies. These waveforms involve elastic-plastic and creep deformations at the crack

tip. These deformations are caused by the cyclic loading at a given frequency and steady loads during a specified hold time [10]. Several studies have shown that creep deformation reduce plasticity-induced crack closure, thus increasing the crack growth rates during the cyclic portion of a creep-fatigue loading waveform. The influence of load ratio R for FCG on P_{OP} has been extensively studied considering crack closure due to plasticity. Several numerical approaches have been developed to simulate crack growth and predict the lifespan of structures. One widely used method is the finite element method (FEM), which involves dividing the structure into small finite elements, applying boundary conditions and loads, and solving for the stress and strain distribution at each node. While other numerical approaches, such as the extended finite element method (X-FEM), strip-yield modeling (SYM), and cohesive zone modeling (CZM) have been developed in the past, this study employs the finite element method.

Sehitoglu et al. [12] and Ramirez et al. [13] employed two-dimensional finite element simulations to study the influence of plasticity-induced crack closure on creep-fatigue crack growth. The study found that the increasing hold time results in larger crack opening displacement (COD) and lower crack-tip opening load, P_{OP} values. Potirniche [14] developed a strip-yield method for predicting crack growth under creep-fatigue loading and found similar effects due to hold times on P_{OP} in several fracture mechanics specimens.

2.4 Variable amplitude loading on FCG and CFCG

While the studies mentioned in section 2.3 focused on FCG and CFCG during CA loading, in practice, engineering structures typically experience variable amplitude (VA) loading. Several researchers have conducted experimental and computational studies to investigate the effects of VA loading in FCG [18-21]. The results showed that overloads produced retardation and underloads produced acceleration of crack growth rates under such loading scenarios. Borrego et al. [19] studied the influence of overload ratio, OLR ($= P_{OL}/P_{max}$), and R -ratio on the post-overload (OL) crack growth rate. They found that the crack growth retardation effect increases with the increased OLR and decreased R -ratio. Gong et al. [22] performed studies of FCG behavior with a single dwell (creep)-overload test on QSTE420TM steel with $R = 0.1$ and $OLR = 2.0$. The retardation degree was not entirely

proportional to the dwell time; its greatest level was recorded when the dwell time was 10^4 s, then it gradually stabilized as the dwell time increased.

Few studies have been performed to date on CFCG behavior under VA loading. Several researchers investigated the effects of overloads on CFCG applied before a hold time during a creep-fatigue cycle. Saarimaki et al. [23] and Pribe et al. [24] found that the detrimental effect of hold times on CFCG can be suppressed or eliminated if an OL is applied before each hold time. The effects of OL depended on both the length of hold and the OLR. To date, no computation study has addressed the influence of creep-fatigue VA loading on plasticity-induced crack closure. The present research study attempts to fill some of this knowledge gap by performing a series of finite element analyses to quantify crack opening loads under VA CFCG loading.

CHAPTER 3: FINITE ELEMENT MODELING

3.1 Specimen geometry and material modeling

The CT specimen is a widely used geometry in fracture mechanics studies. It allows for controlled testing of materials under different loading conditions, such as fatigue and creep-fatigue loading. In this research, a CT specimen with a width of $W = 50$ mm and a thickness of $B = 12.5$ mm was modeled in the commercial software ABAQUS to simulate FCG and CFCG using the finite element method (FEM). The specimen geometry and dimensions are presented in Figure 3 and Table 1, respectively. The specimen dimensions were chosen according to the ASTM E2760 [5] standard on testing methods for CFCG. The specimen used in this study was similar to those used by Ramirez et al. [13] to investigate the effect of plasticity-induced crack closure in CA CFCG loading. Only one-half of the specimen was modeled due to its geometrical and loading symmetries. The initial crack length a was 20 mm, i.e., the crack length to width ratio, a/W was 0.4.

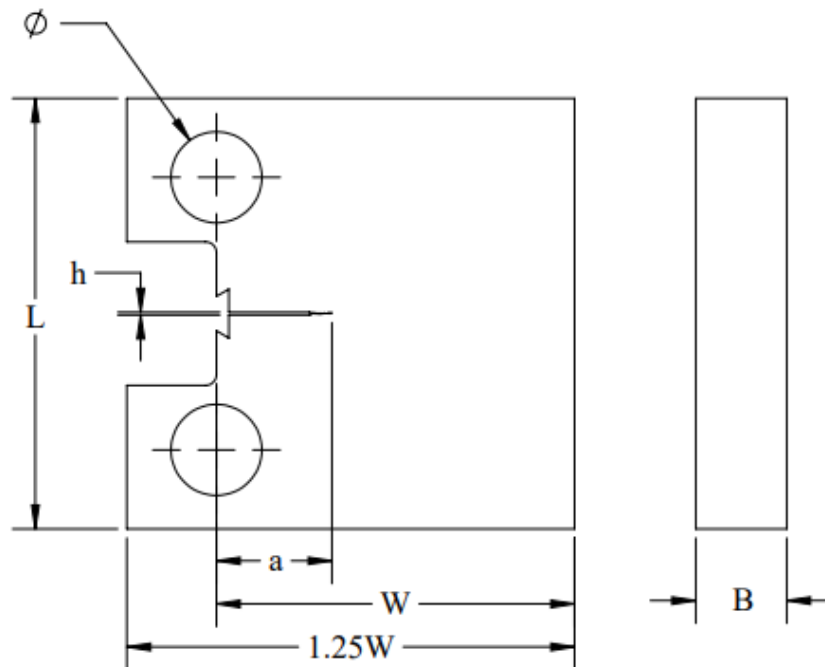


Figure 3. Geometry of the CT specimen used in the finite element simulations.

Table 1. Dimensions for the CT specimen.

Dimensions [mm]	L	W	a	h	Φ	B
	60	50	20	0.5	12.7	12.5

The elastic-perfectly plastic material model is commonly used in finite element simulations to capture the non-linear behavior of materials under loading. In this study, the yield strength was assumed to be equal to the flow stress of the steel, which was determined as the average of the initial yield and flow strength of modified 9Cr-1Mo. The material properties of modified 9Cr-1Mo used in the present study are presented in Table 2 [2, 13]. To model the creep behavior of the material, the strain-hardening version of Norton power law was employed, which is a widely accepted constitutive model for steady-state creep, $\dot{\epsilon}_{cr} = A\sigma^n$.

Table 2. Mechanical properties of modified 9Cr-1Mo.

Material/ Temperature	Young's modulus (GPa)	Poisson ratio	Yield strength (MPa)	Tensile strength (MPa)	Norton creep constant A (MPa) $^{-n}h^{-1}$	Norton creep exponent, n
9Cr-1Mo at 625°C	125	0.3	325	344	9.53E-21	8.24

3.2 Meshing and boundary conditions

The modeled two-dimensional CT specimen was partitioned and structurally meshed with four-node quadrilateral elements of type CPS4R used for simulating plane stress conditions. The partitioning of the specimen is illustrated in Figure 4. To prevent shear locking, reduced integration with hourglass control was employed in the mesh generation

process. The resulting mesh and applied boundary conditions in the two-dimensional CT specimen are presented in Figure 5. The rectangular area of increased mesh refinement was placed around the crack tip to capture the forward and reversed plastic zones around the crack tip, which are critical for the accurate prediction of P_{OP} . The overall mesh is illustrated in Figure 5a, and the most refined region with the largest mesh density is magnified and shown in Figure 5b. The element size in the most refined region was $50\ \mu\text{m}$. The element size was chosen to ensure that on the crack plane ($X = 0$), there were at least 10 elements in the forward plastic zone at maximum load, and at least 3 to 4 elements in the reversed plastic zone at minimum load in the cycle [26, 27]. The total number of nodes and elements generated in the specimen was 11,128 and 10,972, respectively.

Symmetry boundary conditions and constrained displacement were imposed on the finite element mesh. The displacement of all nodes located along the crack plane (from the crack tip to the right side of the specimen) was constrained in the Y -direction ($UY = 0$). Also, the displacement of the load point at the center of the pinhole was constrained in the X -direction ($UX = 0$) [13]. The specimen was loaded on the reference node at the center of the pinhole, where all the nodes around the pinhole diameter were connected via a multiple-point constraint. The applied load was transmitted equally to all the nodes located on the pinhole edge.

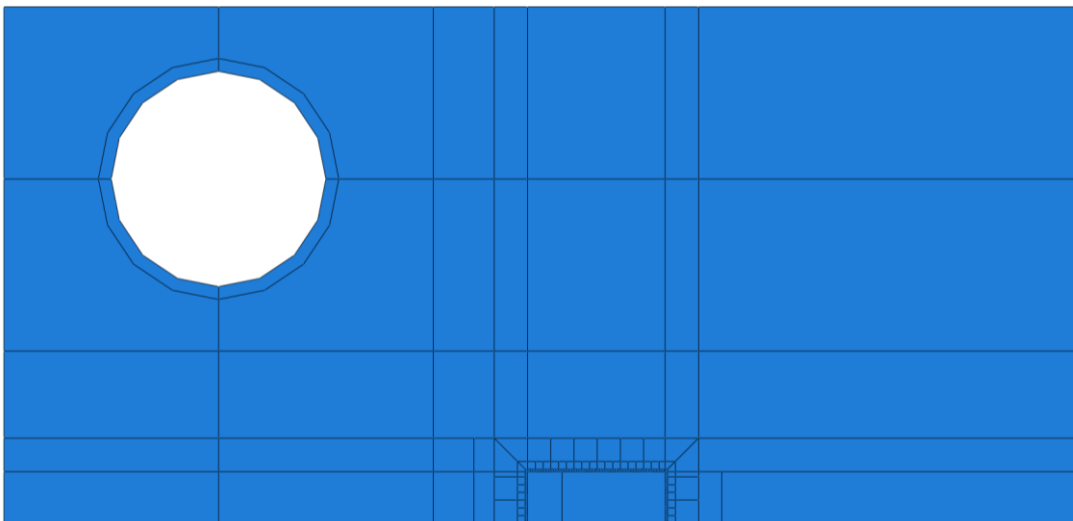


Figure 4. Partitioning of two-dimensional CT specimen.

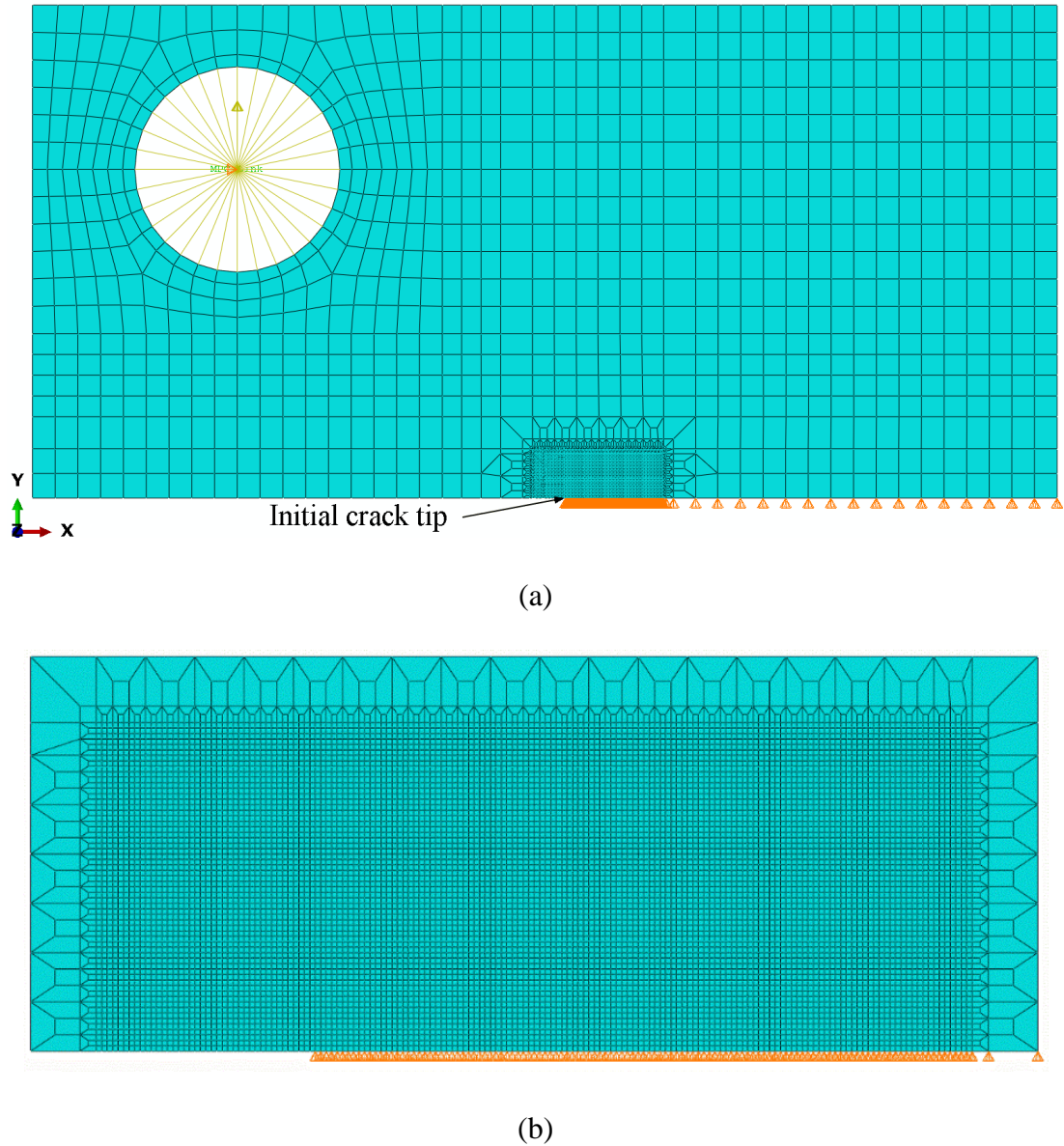


Figure 5. Finite element mesh and boundary conditions for the two-dimensional CT specimen. (a) full specimen mesh, (b) close-up of the most refined region.

3.3 Loading waveforms and crack growth scheme

Several waveforms were considered to study the influence of VA loading on crack opening loads. For the loading portion of each loading cycle, L_T and U_T denote the loading and unloading times, respectively. The duration of load hold time, t_H , in the current simulations, was chosen as either 60 s or 600 s for the creep portion of the CA creep-fatigue

cycle. A total number of 100 cycles were applied to simulate 2.5 mm crack growth for both FCG and CFCG. The load ratio $R = 0.1$ was maintained throughout the simulations during the CA fatigue and creep-fatigue loadings.

OL or underload (UL) was applied in the 41st cycle of the loading waveforms during the crack growth simulations. The total crack growth was 1mm when OL or UL cycle was applied in the simulation. The VA loading waveforms considered in this study are shown in Figure 6. The OLR considered during both FCG and CFCG were 1.10 and 1.15, as shown in Figures 6a and 6b. In CFCG, for the OLR of 1.10 and 1.15, the hold time at OL, t_{OH} , were 60 s, 600 s, and 3600 s. Additionally, fatigue OL during CFCG with an OLR of 2 and 3 was examined and shown in Figure 6c. The underload ratios, ULR ($= P_{UL}/P_{max}$) considered during CFCG were -0.5 and -1 with the underload hold time, t_{UH} , applied at P_{UL} , as shown in Figure 6d. The hold times considered at P_{UL} were similar to those of t_{OH} in Figure 6b.

This study employed the node release method as the crack propagation scheme to simulate plasticity-induced crack closure. In this method, the crack tip node was released every two cycles at minimum load, which entailed removing the node fixity in the Y -direction. The simulated crack propagation resulted from the sequential node release ahead of the crack tip. It is important to note that the crack was advanced by the size of one element in every two cycles, meaning that the method did not reproduce the actual rate of crack growth. Nevertheless, this node release scheme was shown to produce accurate crack-tip opening loads (P_{OP}) for both CA FCG and CA CFCG loading waveforms. The crack opening loads were computed using the node displacement method, which was successfully used in previous studies [13, 28]. In this method, during L_T and U_T , the vertical displacement of nodes behind the crack tip was monitored at each time step. The crack at minimum load was partially closed, resulting in a vertical displacement of zero for some nodes behind the crack tip. The crack remained closed for a portion of the next loading cycle. The remotely applied load at which the first node behind the crack tip opens, i.e., the vertical displacement becomes greater than zero, is defined as P_{OP} . The node release and P_{OP} measurements were performed on alternating cycles to ensure accurate and consistent measurements, as shown in Figure 6a. Notably, this technique was applied consistently across all other loading waveforms, indicated in Figures 6b-6d. The simulation of the contact surface was performed

by utilizing a penalty function or augmented Lagrange algorithm provided in ABAQUS [29] and has been introduced in previous studies [13, 28].

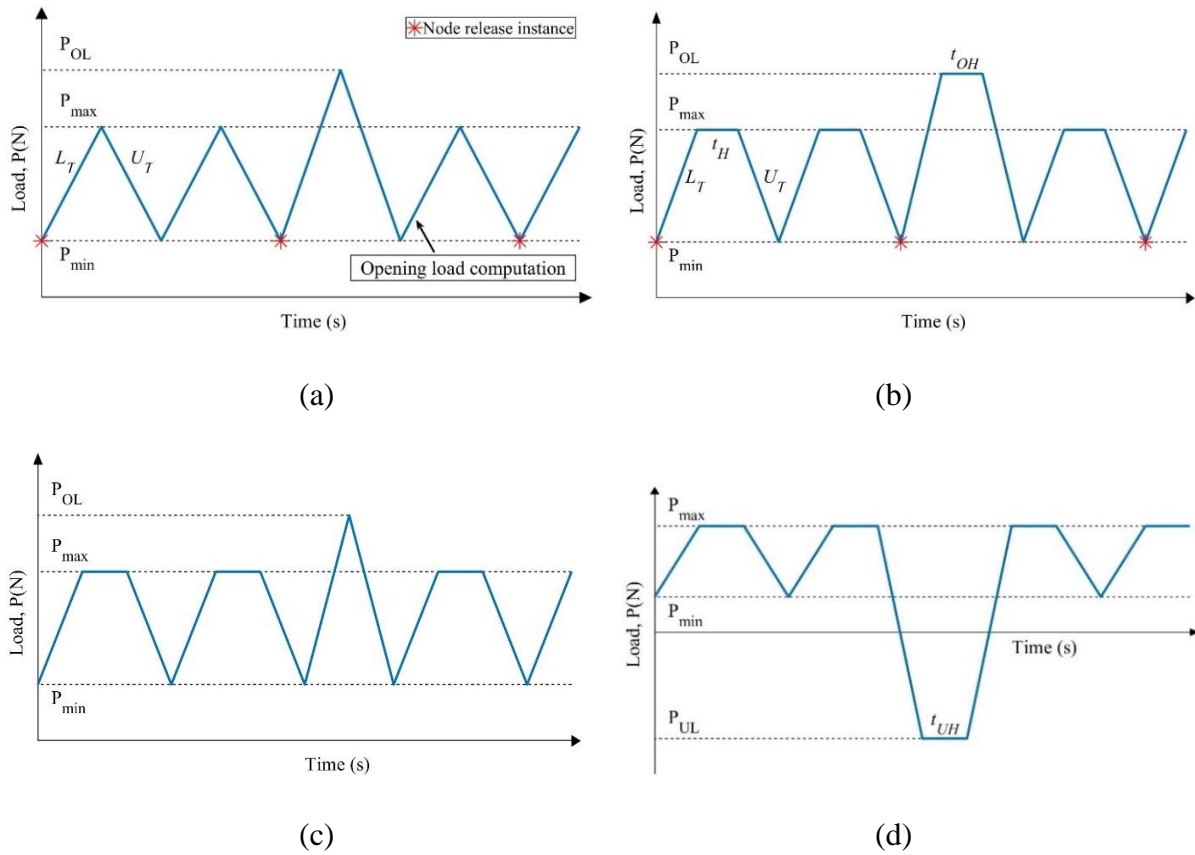


Figure 6. Loading waveforms for (a) Fatigue overload in a FCG cycle, (b) Creep-fatigue overload in a CFCG cycle, (c) Fatigue overload in a CFCG cycle, and (d) Creep-fatigue underload in a CFCG cycle. ($OLR = P_{OL}/P_{max}$ and $ULR = P_{UL}/P_{max}$). Stars indicate the moment when the crack tip node is released.

CHAPTER 4: MODEL VALIDATION

To validate the present finite element (FE) model and simulations, predictions of P_{OP} during CA FCG and CFCG waveforms were compared to the data from published studies that employed both the FEM and SYM techniques [13, 14, 25]. Figure 7 shows the evolution of P_{OP} during FCG from the present model and the previously published study by Ramirez et al. [13]. The two normalized crack opening load P_{OP}/P_{max} curves are almost identical when the same loading conditions were applied in modified 9Cr-1Mo steel at 625°C. In this simulation, the maximum applied load was $P_{max} = 9$ kN and $R = 0.1$. The normalized opening loads initially increased due to the plastic wake build-up behind the crack tip in the initial stage of crack growth. As the plastic wake thickness stabilizes, the opening stresses remain constant after releasing the 25th node, i.e., after the 50 cycles of the applied load. The stabilized value of the opening load P_{OP} is the relevant variable influencing FCG and is analyzed throughout this study.

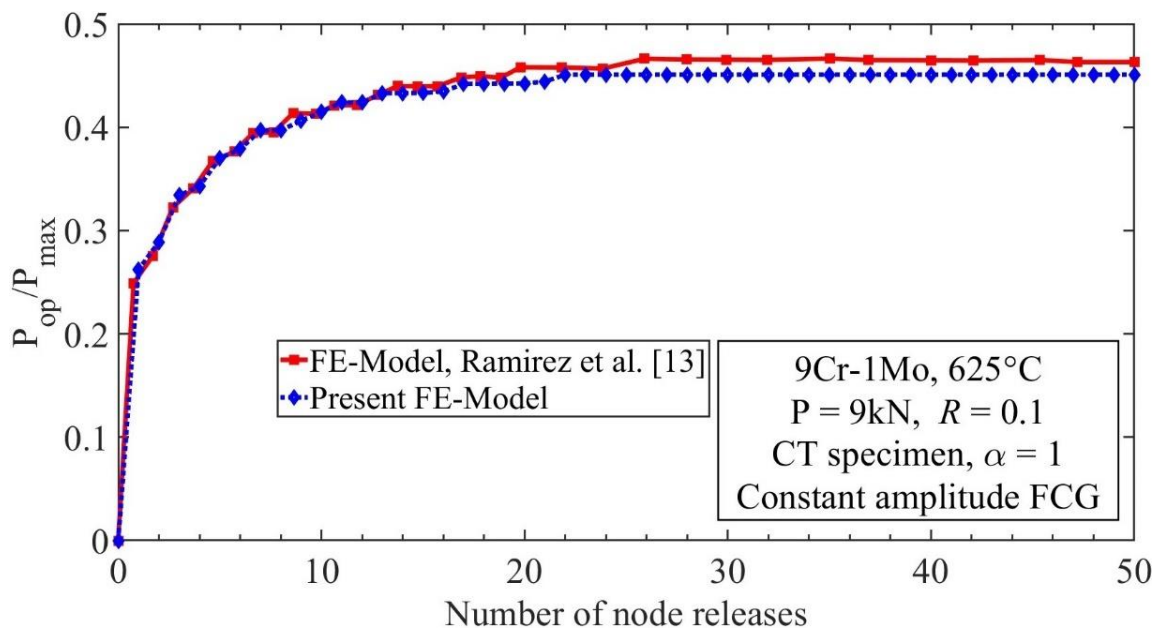


Figure 7. Opening load comparison between the present and previously published data during constant amplitude FCG. (FE = Finite Element)

Figures 8 and 9 present a summary of P_{OP} obtained from this study in the case of CA FCG and CFCG, and comparisons with the previously published data. Figure 8 shows the stabilized P_{OP} for R -ratios ranging between -2 and 1 during CA FCG. The normalized P_{OP} values from the present model are in good agreement with the published data when the R ratio is between 0 and 0.7. For the negative R ratios, there is also good agreement between the present model and a previous FE model [13], while minor differences are recorded between this study and data obtained from SYM simulations [14,25].

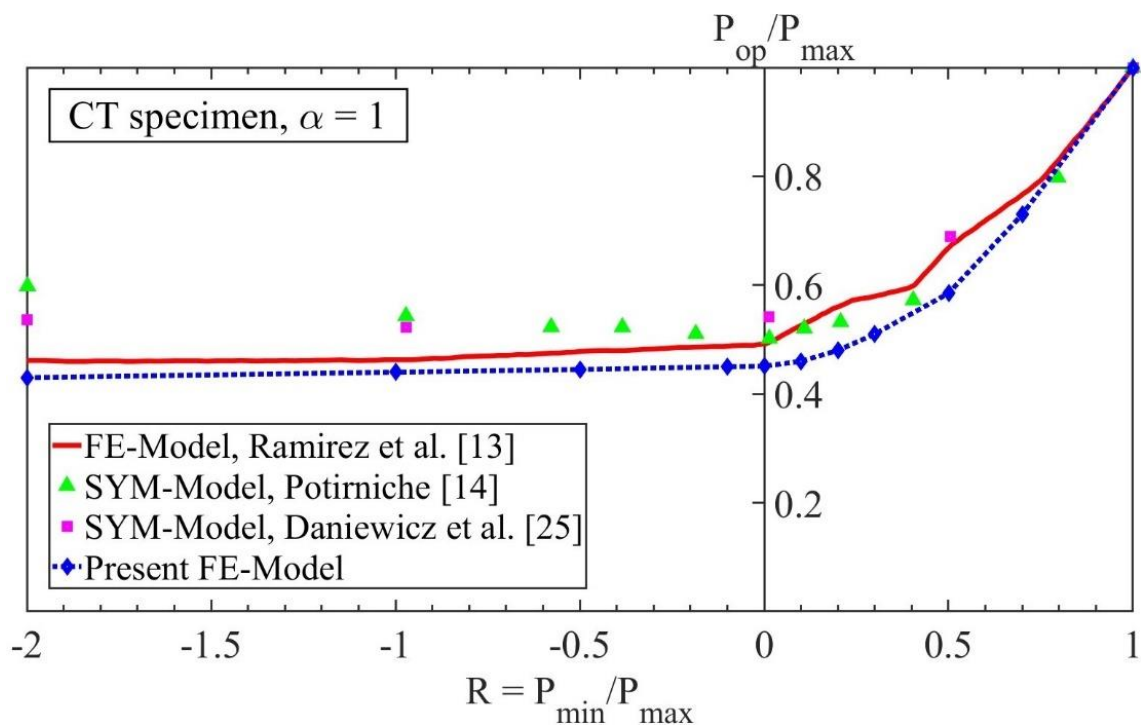


Figure 8. Predictions of normalized opening loads during constant amplitude FCG for different load ratios. (FE = Finite Element, and SYM = Strip-Yield Modeling)

The variation of normalized crack opening loads for increasing ΔK during CA FCG and CFCG are presented in Figure 9. Excellent agreement is obtained for the normalized opening loads during CFCG with $t_H = 0$ s in the present model and the published data [13]. In general, the results also agree with slight differences in the case of CFCG with $t_H > 0$ when compared with the data from the same study. The opening loads decreased with an increasing

hold time at maximum load and with increasing ΔK . All three opening load curves decreased to the minimum load of $0.1P_{max}$ because the crack remained open at the minimum load with higher ΔK and large hold times. Since the computed crack opening loads during both FCG and CFCG agree with the published data, it can be concluded that the present model and all the numerical simulation details are properly set up for the prediction of crack opening loads during VA FCG and CFCG.

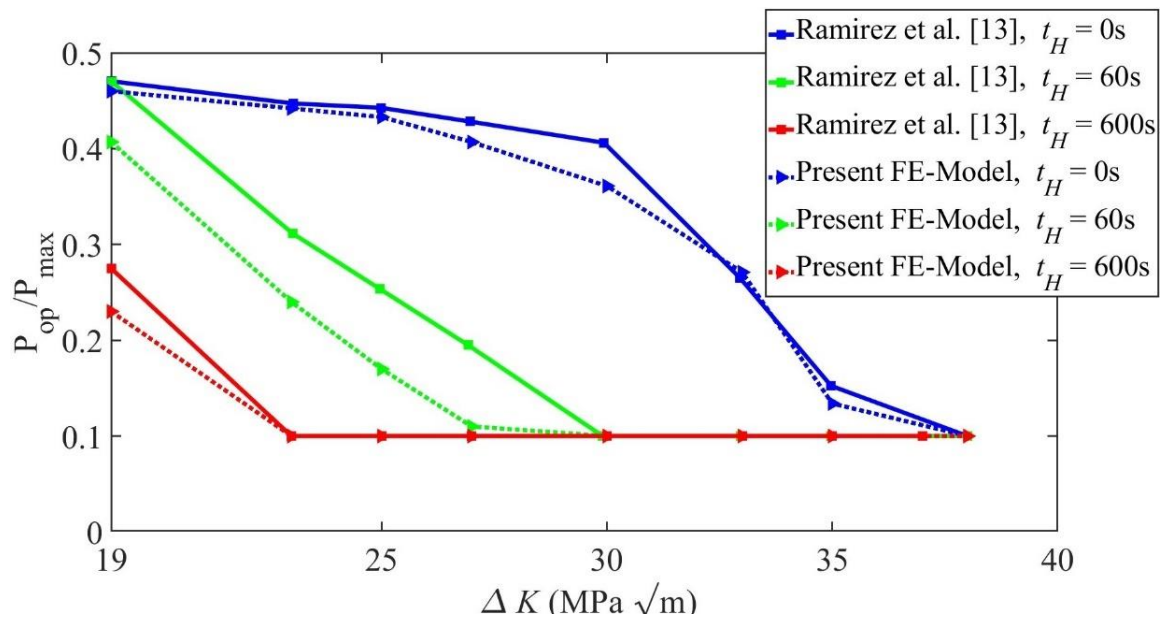


Figure 9. Variation of crack-tip opening loads with ΔK during CA CFCG with different hold times.

CHAPTER 5: RESULTS AND DISCUSSION

5.1 Constant amplitude loading during CA FCG and CFCG

The evolution of normalized crack opening load curves during CA FCG and CFCG is presented in Figure 10. The crack-tip opening load is the level required to open the crack tip slightly and initiate crack growth during each cycle. The three different curves on this plot correspond to different hold times, i.e., the fatigue loading case with $t_H = 0$ s, and two creep-fatigue loading cases with $t_H = 60$ s and $t_H = 600$ s. This figure shows the effect of creep hold time on crack opening. The decrease in crack-tip opening loads is proportional to the increase in applied hold time at the maximum load in the CFCG cycle.

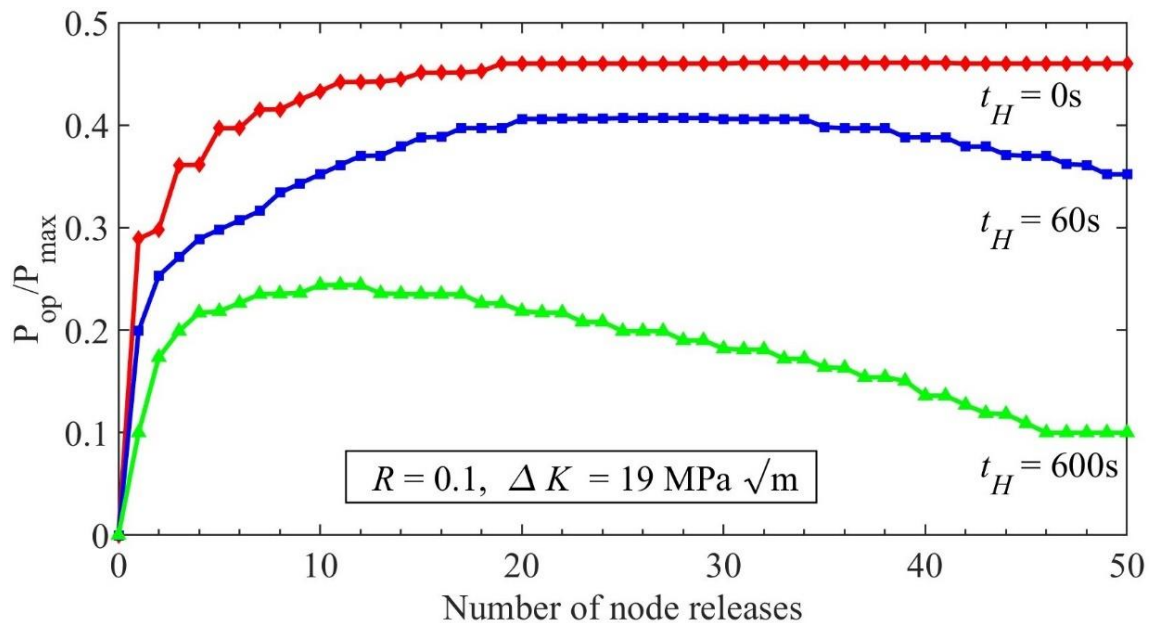
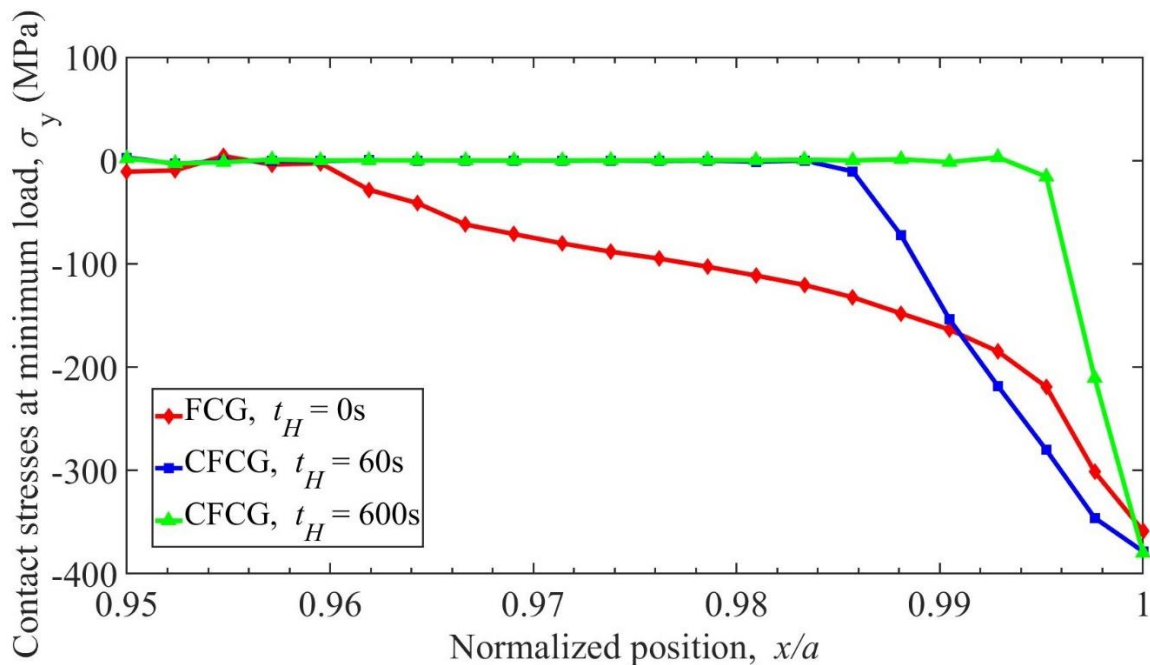


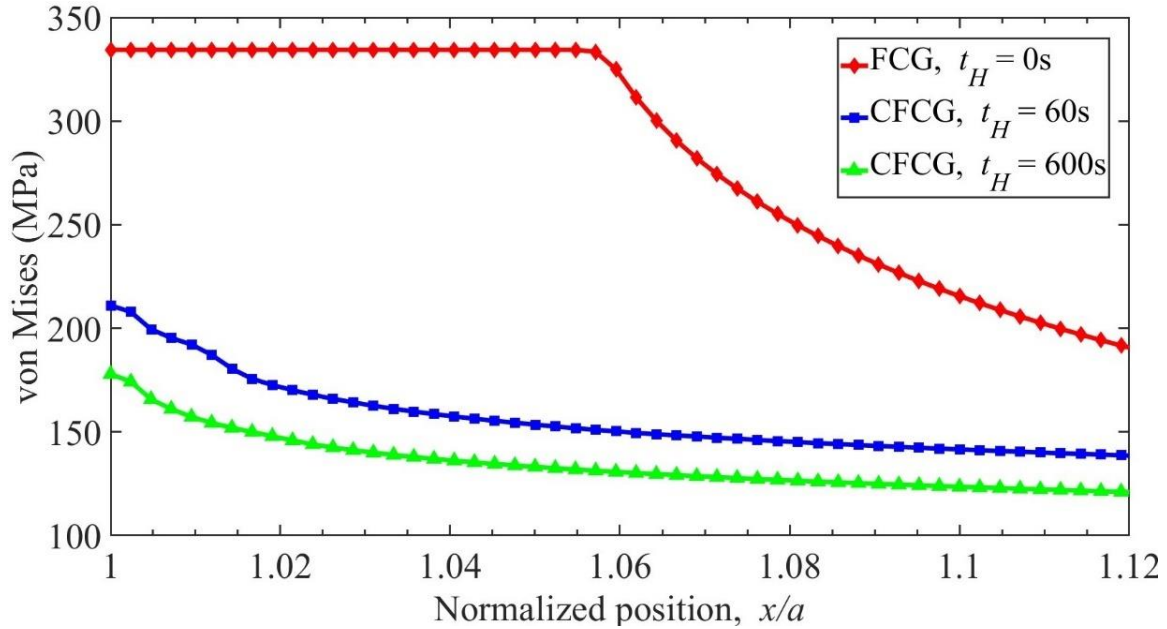
Figure 10. Normalized crack opening loads during constant amplitude FCG and CFCG for $t_H = 60$ s and $t_H = 600$ s.

Figure 11a shows the variation of contact stresses between the crack surface behind the crack tip at minimum load, and Figure 11b shows the stress distribution of the von Mises

equivalent stress ahead of the crack tip at maximum load after hold time during cycle 41. The crack growth during cycle 41 was 1 mm. From Figure 11a, it can be observed that the longer the hold time, the lower the contact compressive stresses between the crack surfaces. This is explained by the accumulation of creep strain ahead of the crack tip, leading to increased crack opening, thus reducing the amount of crack closure at minimum load. Additionally, in the front of the crack tip, the equivalent stress relaxes with increasing creep time. During load hold time, the creep deformation induces stress relaxation and crack tip blunting. Once the crack-tip deformation and blunting stabilize at the crack-tip, further increase in crack-tip opening loads is impeded. Therefore, the creep deformation at the crack tip increased the crack-tip opening displacements at the maximum load, and decreased the crack-tip opening loads.



(a)



(b)

Figure 11. (a) Contact stresses behind the crack tip at minimum load in cycle 41, and (b) equivalent von Mises stresses ahead of the crack tip at maximum load in cycle 41 after hold time. The crack tip is located at position $x/a = 1$, where a is the crack length.

Figure 12 presents contour plots of the equivalent plastic strain (PEEQ) and creep strain (CEEQ), in the region surrounding the crack tip, during cycle 41, or between node releases 20 and 21. Figures 12a and 12b compare the PEEQ fields, and Figures 12c and 12d compare the CEEQ between a case of CFCG loading with a hold time $t_H = 60$ s and $t_H = 600$ s, respectively under CA loading. From Figures 12a and 12b, it can be observed that the crack develops a constant thickness plastic wake for each hold time. The creep zone size and creep strain magnitude increase in the crack-tip region with increasing load hold time t_H , as shown in Figures 12c and 12d. The crack opening displacement (COD) behind the crack tip is much larger in Figures 12b and 12d when compared with those in Figures 12a and 12c which is caused by the longer hold times applied in the CA cycles ($t_H = 600$ s versus $t_H = 60$ s).

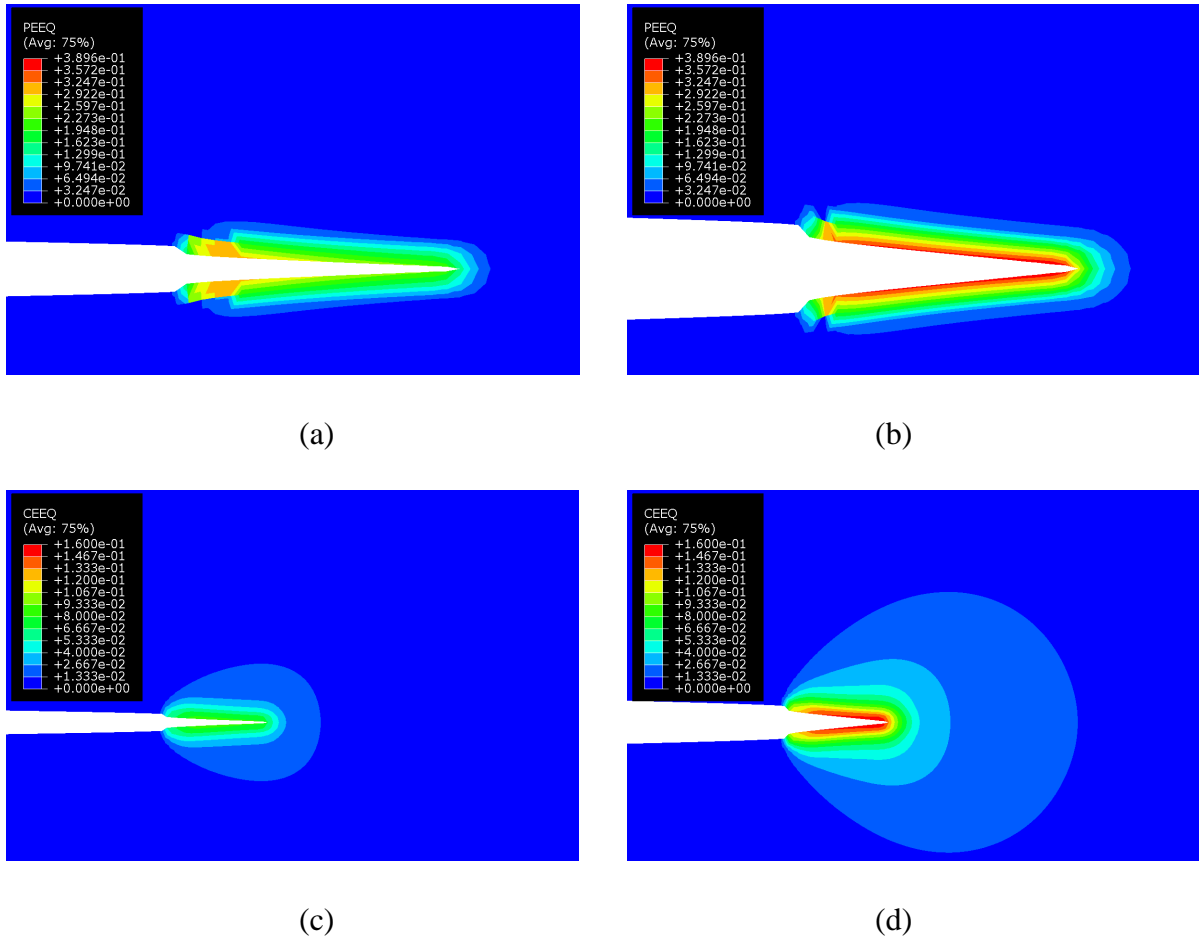


Figure 12. Crack-tip region during CA CFCG with hold times in cycle 41 in (a) $t_H = 60$ s, (b) $t_H = 600$ s, (c) $t_H = 60$ s, and (d) $t_H = 600$ s. Contour plots of equivalent plastic strains (PEEQ) in (a) and (b), equivalent creep strains (CEEQ) in (c) and (d). The deformation scale factor is

4.

After plasticity near the crack tip region stabilizes, the creep deformation continues to accumulate at the crack tip and further decreases the crack opening loads. The decreasing trend of crack-tip opening loads after relative stabilization during CFCG can be seen in Figure 10. Also, it can be observed that the decreasing trend in the curve for $t_H = 600$ s starts in an early cycle compared to that for $t_H = 60$ s since the increase in hold time at maximum load increases the COD at the crack tip. Hence, the stabilized crack opening loads during $t_H = 600$ s were reduced, and the decreasing trend started early in the loading cycle.

5.2 Single overload cycle during FCG

The variation of crack opening loads during VA FCG is shown in Figure 13. The curves in the figure represent the CA FCG, and two FCG with a single overload case with $OLR = 1.10$ and $OLR = 1.15$. The applied loading waveform for VA FCG in the finite element simulations corresponds to Figure 6a. The OL was applied in the 41st cycle of the crack growth simulation. As a result of the single OL cycle, a perturbation in the plastic deformation occurred at the crack tip, which is proportional to the magnitude of OLR. The initial drop in the crack-tip opening load is due to the increased maximum load during the OL, which led to an increased crack-tip opening displacement compared to that during CA loading. Hence the sharp decrease in the crack opening load after the OL cycle, which is illustrated in Figure 13.

At the same time, the OL produced a large plastic zone ahead of the crack tip. In the loading cycles after the application of the OL, the crack tip propagates through the larger plastic zone size, and the plastic wake builds up slowly to a thickness that eventually becomes larger than that during CA loading. This explains the increasing trends of the opening load after the initial dip caused by the OL. The opening loads increase to a level larger than that measured during CA loading only after a few load cycles after the OL. It can be concluded that the OL overall leads to a reduction in the crack growth rate for this level of OLR, as the opening load level increases and the crack is shielded by a thicker plastic wake [22].

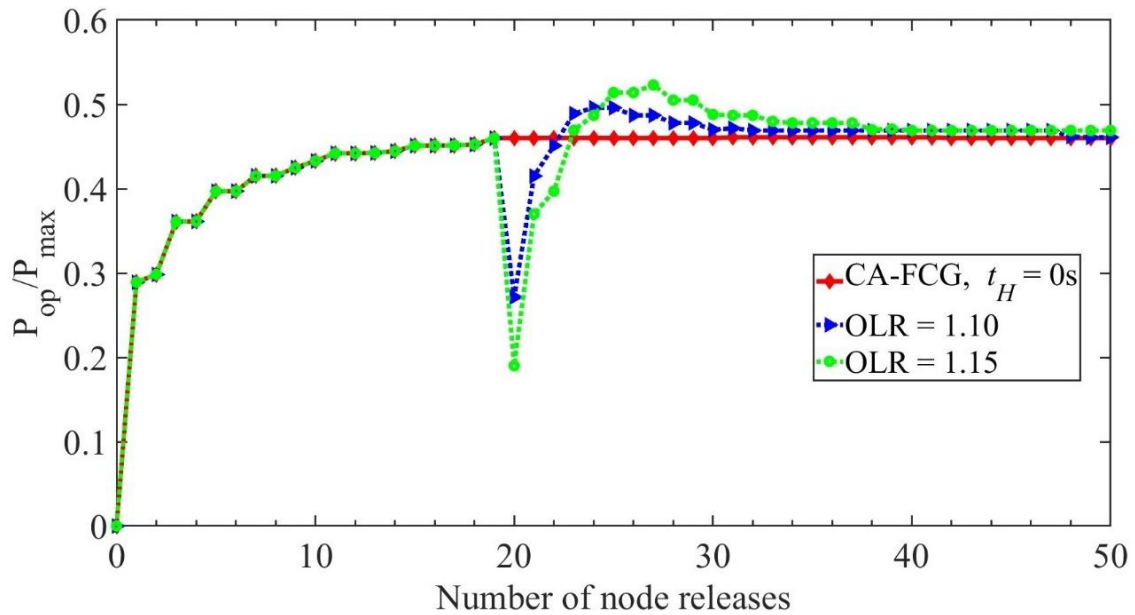


Figure 13. Single overload effect on crack-tip opening loads during CA FCG.

Figure 14 presents contour plots of the PEEQ, in the region surrounding the crack tip, during cycle 41 (OL cycle) and cycle 58 (between node releases 29 and 30). Figures 14a and 14b compare the PEEQ fields in cycle 41 during the CA loading and VA loading in FCG. The crack growth during cycle 41 was 1 mm. It can be observed that the plastic zone and COD are larger at the crack tip due to OL in Figure 14b. Figures 14c and 14d compare the PEEQ fields in cycle 58 during the CA loading and VA loading. The crack growth during cycle 58 was 1.45 mm. The crack propagated through a larger plastic zone and the plastic wake thickness is larger in Figure 14d than in Figure 14c.

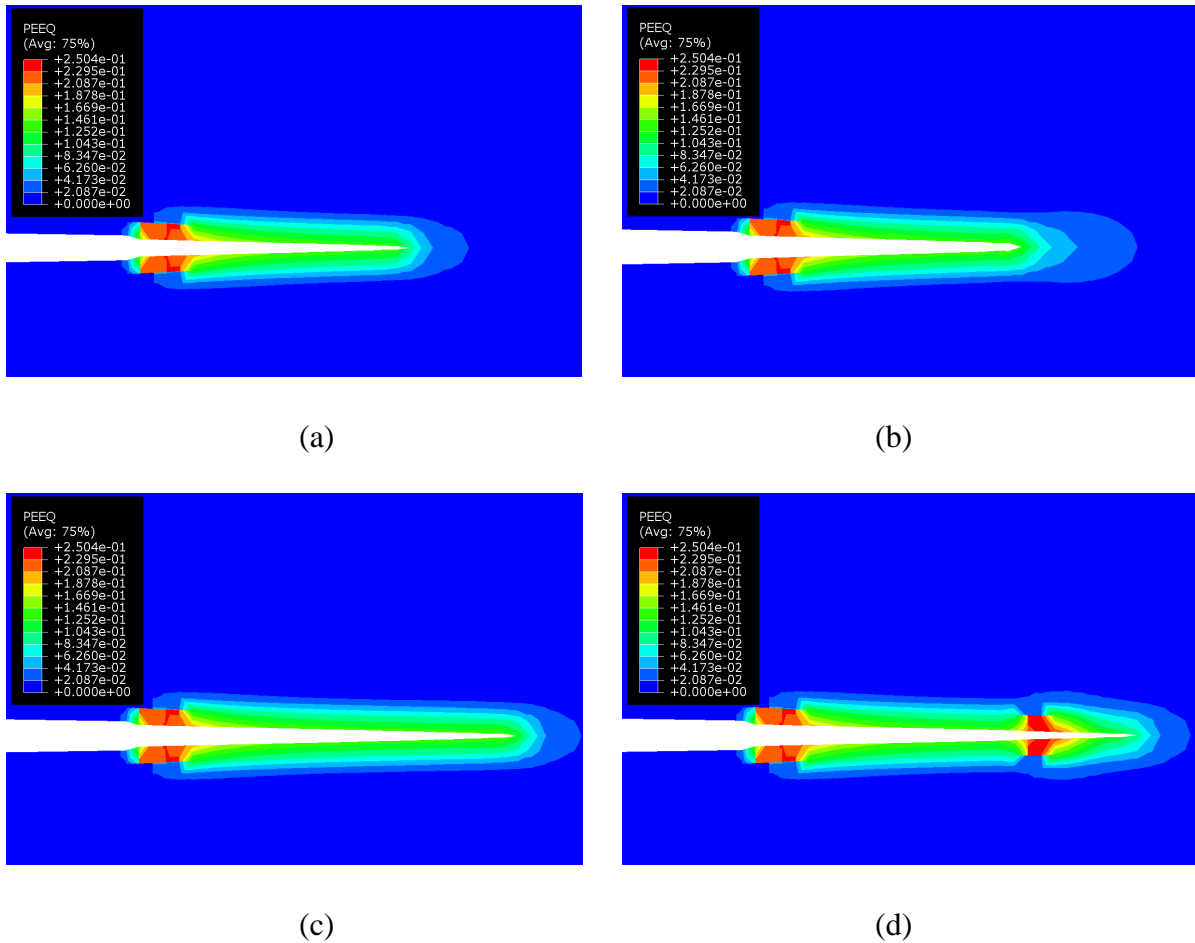


Figure 14. Contour plots of equivalent plastic strains in cycle 41 in (a) CA FCG and (b) OLR = 1.15 in FCG, and in cycle 58 in (c) CA FCG and (d) OLR = 1.15 in FCG. The deformation scale factor is 4.

5.3 Variable amplitude loading during CFCG

5.3.1 Single creep-fatigue OL

This section summarizes the results of creep-fatigue OL during CFCG. A single creep-fatigue OL with OLR 1.10 and 1.15 was applied in the 41st cycle during the CFCG with $t_H = 60$ s. The hold time, t_{OH} , at maximum load in the OL cycle was 60 s, 600 s, and 3600 s. The loading waveform applied in these cases corresponds to Figure 6b. The influence of creep-fatigue OL during CFCG on crack opening loads is presented in Figure 15. From

this figure, it can be observed that for both the initial drop in opening load and subsequent build-up to larger opening load P_{OP} . Similarly to the case discussed in the previous section on VA FCG loading, in the case of VA CFCG loading, the opening load decreased suddenly after the application of the OL. The decrease is larger with larger OL, which indicates that the drop is caused by the larger crack-tip opening displacements caused by the OL. The trend in opening load then increases slowly to values larger than those recorded for the CA loading case. This is due to the accumulation of inelastic strains (both plastic and creep) ahead of the crack tip, which leads to a steady increase in the plastic wake thickness and increased shielding of the crack tip after the application of the OL. From this plot, it can be concluded that the crack growth is overall slowed down with the application of a single OL during CFCG. The decrease in the crack growth rate is larger with a larger OLR and longer hold time.

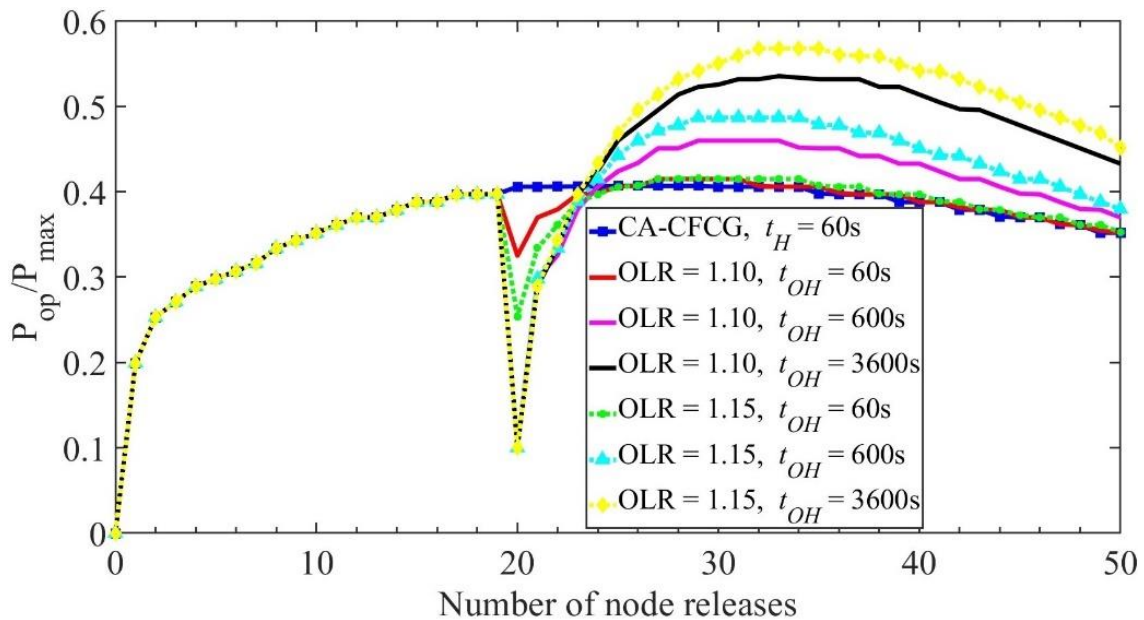
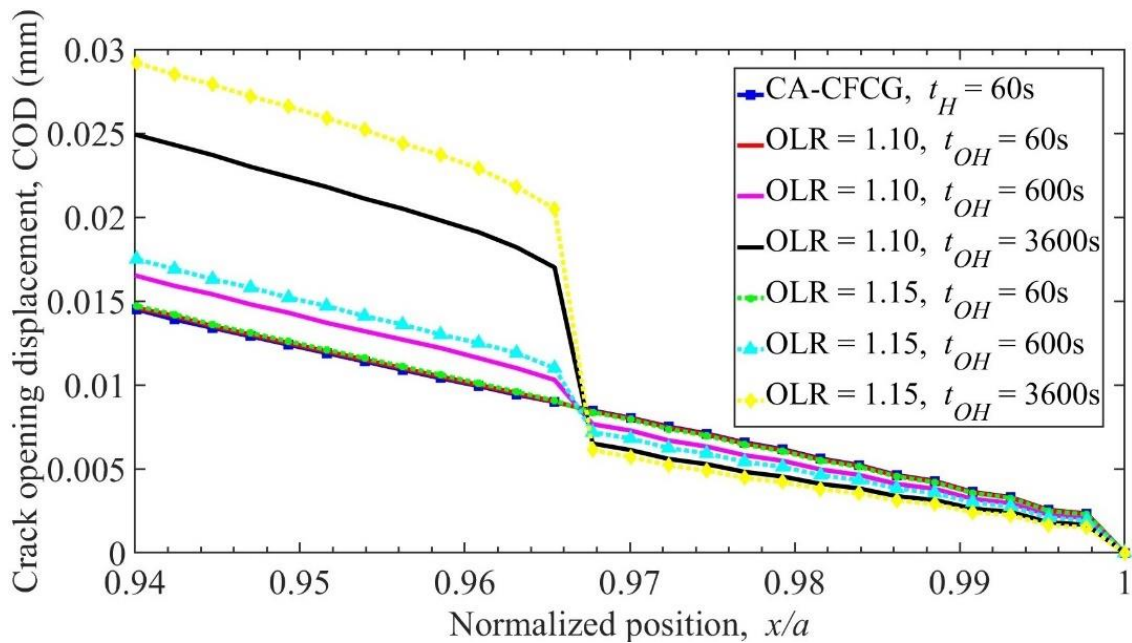


Figure 15. Effects of single creep-fatigue overload on crack opening loads during CFCG.

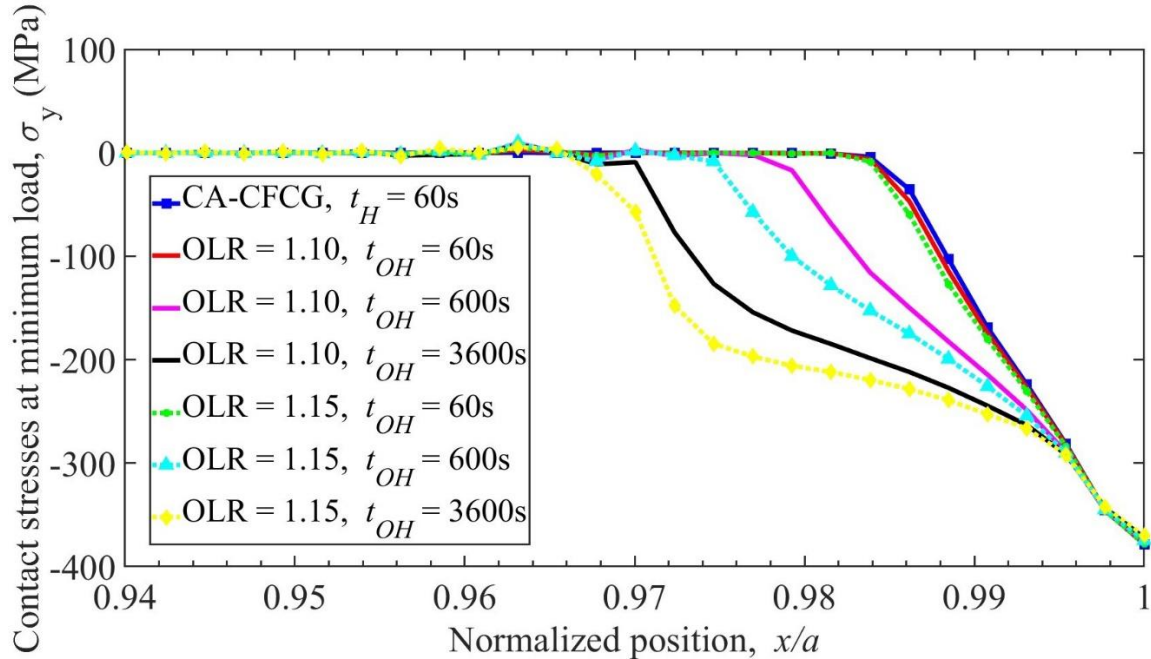
Figure 16 presents details on the crack opening and closing mechanics that explain the observed trends on crack-tip opening loads. From Figure 16a, it can be observed that the longer the hold time applied in the OL cycle, the bigger the increase in the crack-tip opening

displacement in cycle 69 (between node releases 34 and 35), when the OL was applied. The crack growth during cycle 69 was 1.7 mm. This explains the sudden drop in the P_{OP} . Immediately after the OL application, the crack-tip displacement drops off to values much lower compared to those before the OL. The OL causes a larger plastic zone ahead of the crack tip. The crack-tip opening displacement decreases as the crack propagates through the increased forward plastic zone. The larger the OL value, the lower the crack-tip opening displacement, and, consequently, the higher the crack-tip opening load caused by the OL. This, in turn, leads to a reduction in the crack growth rate, as an increased crack-tip opening load results in a lower value of ΔK_{eff} .

Figure 16b shows the variation of the contact stresses at the minimum load in cycle 69 during the CA and VA creep-fatigue loading waveforms. It can be observed that the contact stresses behind the crack tip are negative, signifying that the crack is closed at minimum load. The increase in the compressive contact stresses behind the crack tip is proportional to the OLR and t_{OH} in the OL cycle. Hence, due to the large creep deformation at the crack tip during the OL cycle, the compressive contact stresses increased in the post-OL cycles, causing in turn, an increase in the crack-tip opening loads.



(a)



(b)

Figure 16. Effects of single creep-fatigue overload in cycle 69 (between node releases 34 and 35) on the (a) crack opening displacement and (b) contact stresses, behind the crack tip crack-tip. The crack tip is located at position $x/a = 1$, where a is the crack length.

Figures 17 and 18 present contour plots of the PEEQ and CEEQ, in the region surrounding the crack tip, during cycle 69, or between node releases 34 and 35. Figures 17a and 17b compare the PEEQ fields between a case of CFCG loading with a hold time $t_H = 60$ s under CA loading (Figure 17a) and VA loading in cycle 69 with OLR = 1.15 and $t_{OH} = 3600$ s (Figure 17b). The OL is applied in cycle 41 (node release 20). In Figure 17b, it can be observed that a perturbation in the smoothness and a thickening of the plastic wake are caused by the application of the OL. In addition, the overall opening of the crack increases due to the larger creep hold time applied in the OL cycle. A similar effect is observed when Figure 17d is compared with Figure 17c. Figure 17c shows the PEEQ plastic wake behind the crack tip for CA CFCG loading with $t_H = 600$ s. By comparison, Figure 17d shows the PEEQ plastic wake when an OL is added in cycle 69 to the waveform resulting in the case illustrated in Figure 17c. A significant thickening of the plastic wake can be observed after

the OL is applied, which results in an increase in crack-tip opening load, as demonstrated in Figure 15, node release 35.

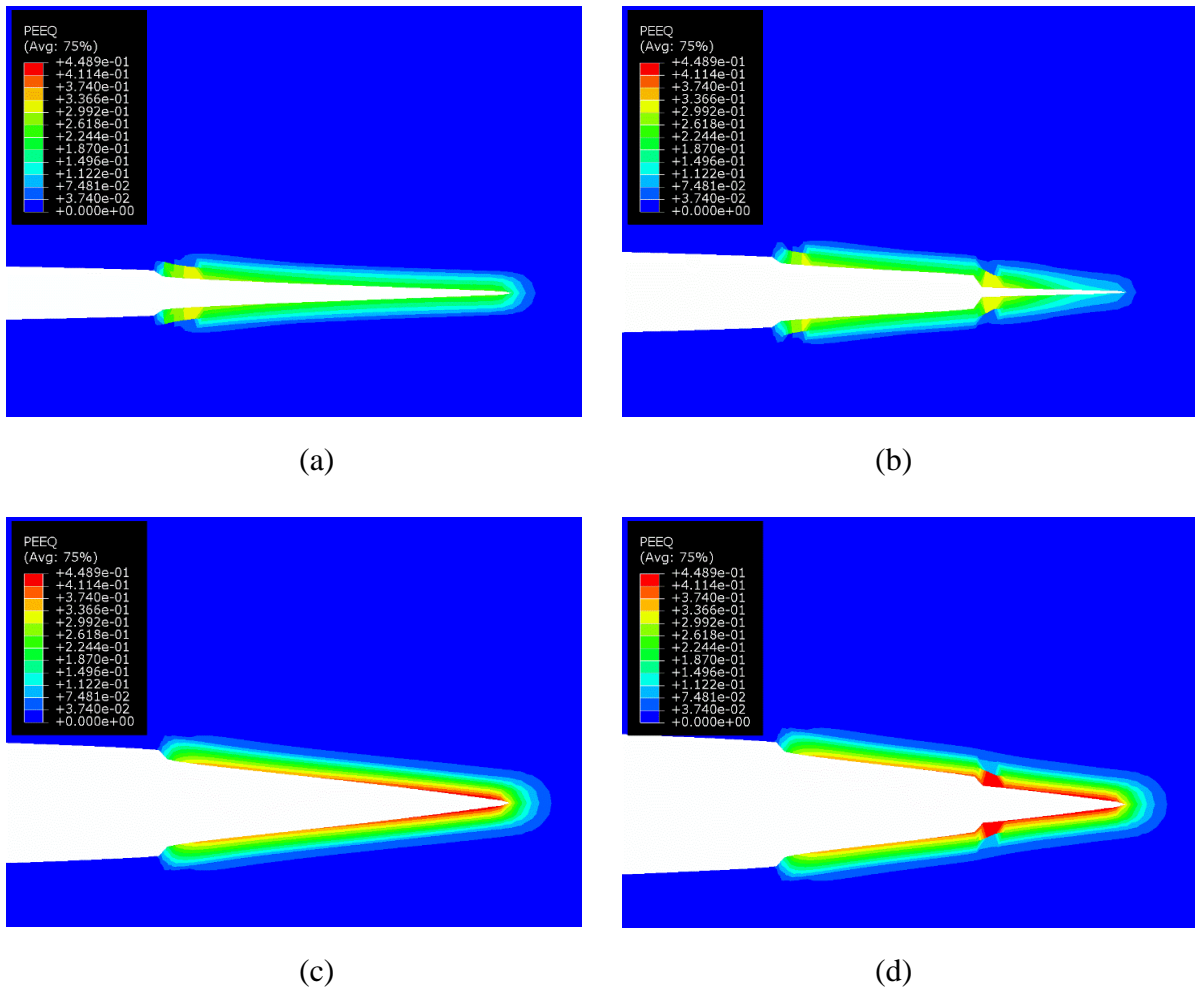


Figure 17. Contour plots of equivalent plastic strains in cycle 69 after hold time during (a) constant amplitude CFCG, $t_H = 60$ s, (b) OLR = 1.15 and $t_{OH} = 3600$ s in CFCG with $t_H = 60$ s (c) constant amplitude CFCG, $t_H = 600$ s, and (d) OLR = 1.15 and $t_{OH} = 3600$ s in CFCG with $t_H = 600$ s. The OL is applied in cycle 41 (node release 20). The deformation scale factor is 4.

Figure 18 shows the CEEQ contour plots for the same loading scenarios represented in Figure 15. Figure 18a shows the CEEQ for a CA CFCG loading waveform with $t_H = 60$ s.

By comparison, in Figure 18b, CEEQ contours are shown for a case when an OL with $OLR = 1.15$ and $t_{OH} = 3600$ s is added to the CA loading waveform in cycle 69. The largest CEEQ values are recorded at the location of the crack tip during cycle 41 (node release 20) when the OL is applied. The OL creates a sudden increase in the creep strain zone ahead of the crack tip at the moment when the OL was applied. After cycle 41, the creep zone ahead of the crack tip decreases in magnitude narrowing toward the crack tip. The COD is larger in Figure 18b compared to that in Figure 18a due to the larger creep hold time applied during the OL. Figures 18c and 18d compare the case of CA CFCG loading with $t_H = 600$ s and the case when an OL cycle with $OLR = 1.15$ and $t_{OH} = 3600$ s is introduced in cycle 41 (node release 20). Similarly, to the case in Figure 18b, the largest CEEQ is recorded at the moment when the OL is applied. After the OL application, the CEEQ zone does not decrease as significantly as in the case of Figure 18b. The thickness of the CEEQ creep wake is larger in the case of Figure 18d compared to that in Figure 18c.

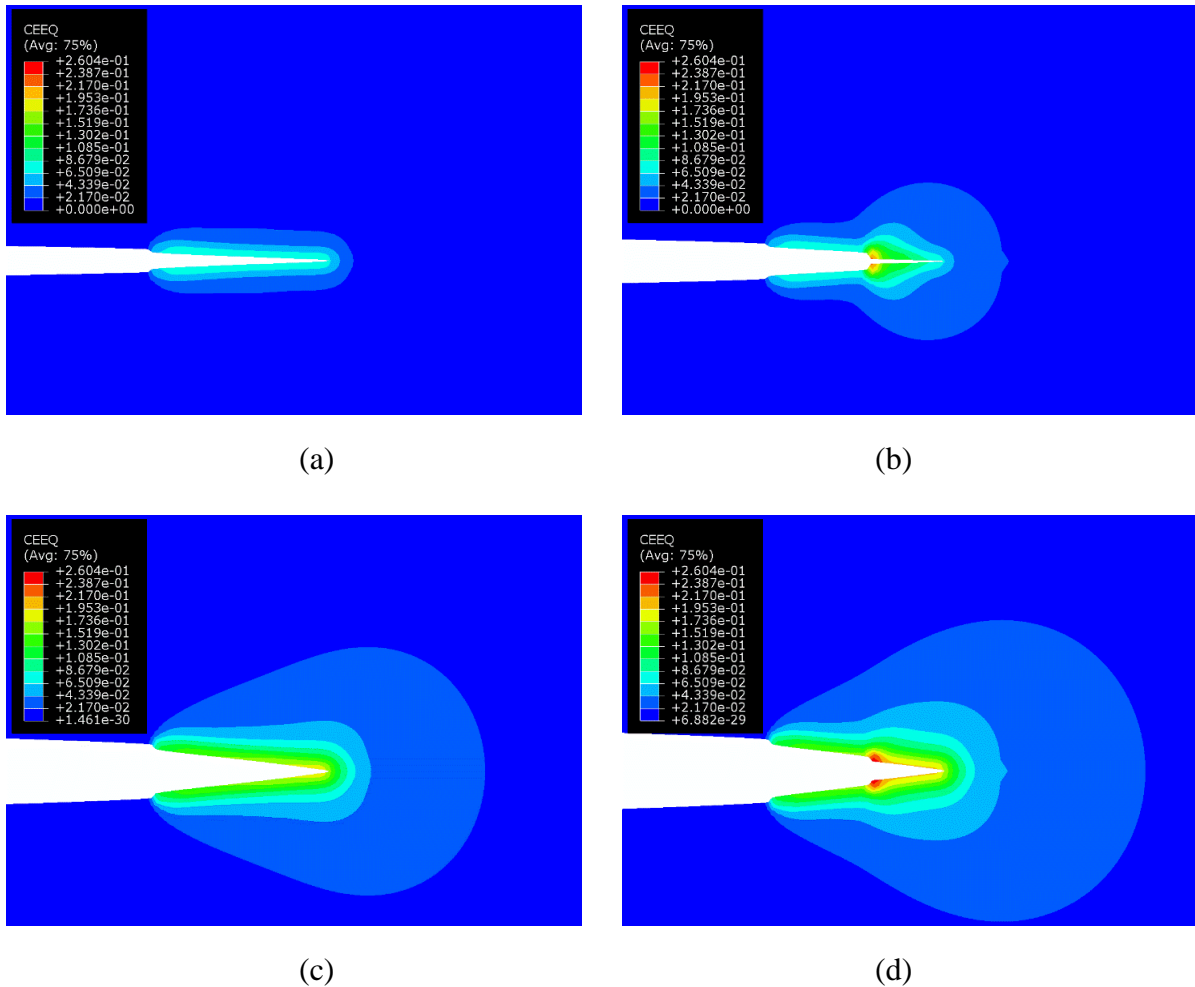


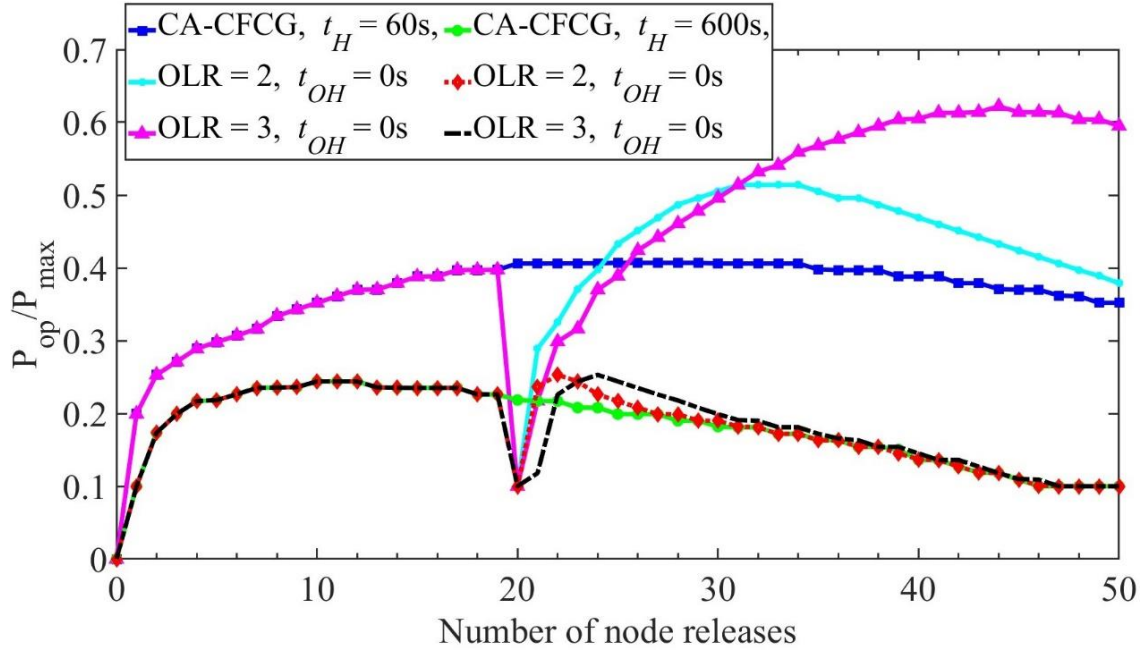
Figure 18. Contour plots of equivalent creep strains in cycle 69 after hold time (a) constant amplitude CFCG, $t_H = 60$ s, (b) $OLR = 1.15$ and $t_{OH} = 3600$ s in CFCG with $t_H = 60$ s (c) constant amplitude CFCG, $t_H = 600$ s, and (d) $OLR = 1.15$ and $t_{OH} = 3600$ s in CFCG with $t_H = 600$ s. The OL is applied in cycle 41 (node release 20). The deformation scale factor is 4.

5.3.2 Single fatigue OL

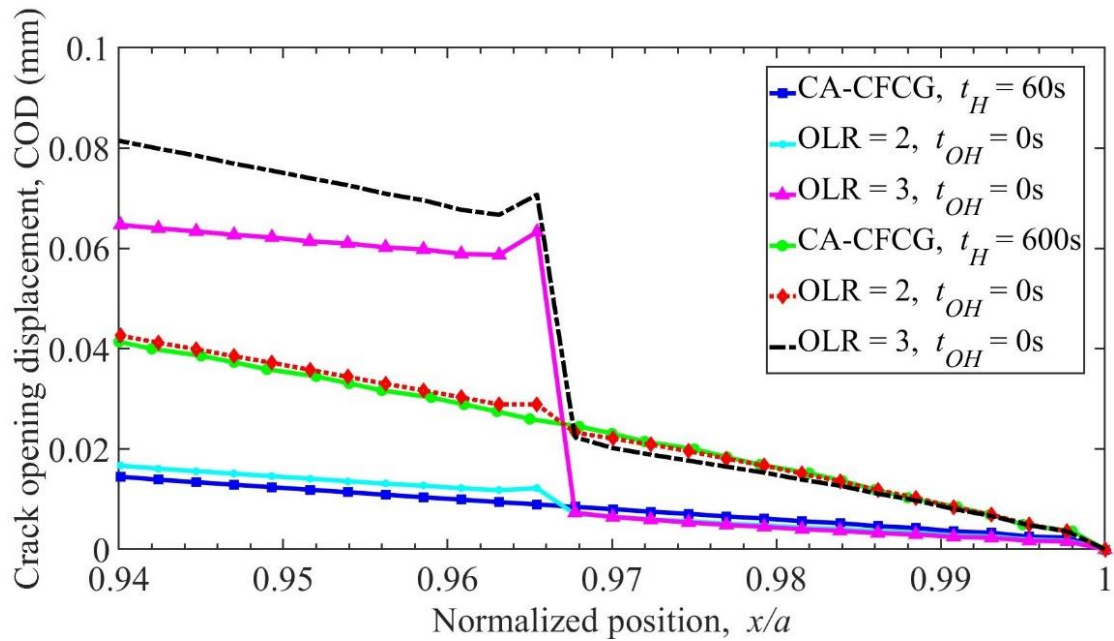
This section presents the crack-tip opening load, COD, and contour plots for PEEQ and CEEQ when a single fatigue OL cycle with OLR of 2 or 3 is applied in a CA CFCG waveform with $t_H = 60$ s or 600s. The loading waveform applied for single fatigue OL during the CFCG simulations is shown in Figure 6c. The crack opening load behavior due to single fatigue OL cycle in the post-OL cycles are presented in Figure 19a. First off, when comparing the opening loads for CA CFCG with either $t_H = 60$ s or $t_H = 600$ s, it can be

observed that the crack-tip opening loads decrease with an increase in the hold time t_H . When a fatigue OL cycle is introduced, the opening loads record a sudden drop due to the large COD caused by the increase in the load level during OL. The plastic deformation at the crack tip during the OL cycle is proportional to the magnitude of OLR, while the COD in the post-OL cycles are not affected by the fatigue OL as shown in Figures 19b and 20. The plastic wake and the crack opening loads continue to build up in the post-OL cycles to values larger than those corresponding to CA waveform. The same overall trend in opening loads is observed for both hold times, however, it can be noticed that the OL has a greater impact in the case of $t_H = 60$ s than $t_H = 600$ s. As the opening load decreases due to the larger applied t_H in the CA CFCG cycles, the impact of a fatigue OL is diminished. Another observation from these simulations is that the amount of OLR plays a significant role in determining the increased values of opening loads and corresponding crack growth retardation in the post-OL cycles. The larger the OLR, the greater the crack-tip opening load and crack growth retardation effects in the post-OL cycles.

Figure 19b plots the CODs in cycle 69 when a single fatigue OL is applied in cycle 41 (node release 20). The crack growth during cycle 69 was 1.7 mm. For CA CFCG loading, the COD is larger when $t_H = 600$ s compared to when $t_H = 60$ s. In the case of a single fatigue OL with $OLR = 2$, the COD does not indicate a significant difference when compared to the case of a CA loading. When $OLR = 3$ in the fatigue OL cycle, the CODs become much larger than those in the CA loading case. Eventually, after several cycles post-OL, the COD returned to its CA loading trend.



(a)



(b)

Figure 19. Effects of single fatigue overload on (a) crack opening loads during CFCG with hold times 60 s and 600 s (b) crack opening displacements in cycle 69 after hold time. The crack tip is located at position $x/a = 1$, where a is the crack length.

Figure 20 indicates the contour plots for PEEQ and CEEQ by comparing the case of CA loading versus the case when a single OL cycle with $OLR = 2$ is applied in cycle 41. The contour plots are captured in cycle 69 of crack growth. Figure 20a shows a constant thickness of the crack plastic wake represented by the PEEQ map. In Figure 20b, the OL is applied in cycle 41. A localized increase in the PEEQ values is observed at the location where the crack tip was when the OL was applied. After the OL, the crack develops a plastic wake with a larger thickness than in the case of CA loading, signifying increased opening loads and crack growth retardation.

Figures 20c and 20d compare the CEEQ contour plots for the case of CA loading versus the case when a single fatigue OL cycle with $OLR = 2$ is inserted in the CA loading waveform. It can be observed that in general, the most intense creep strains located near the crack plane do not exhibit a significant disturbance when an OL is applied. The thickness and extent of the intense CEEQ region remain approximately the same when Figures 20c and 20d are compared.

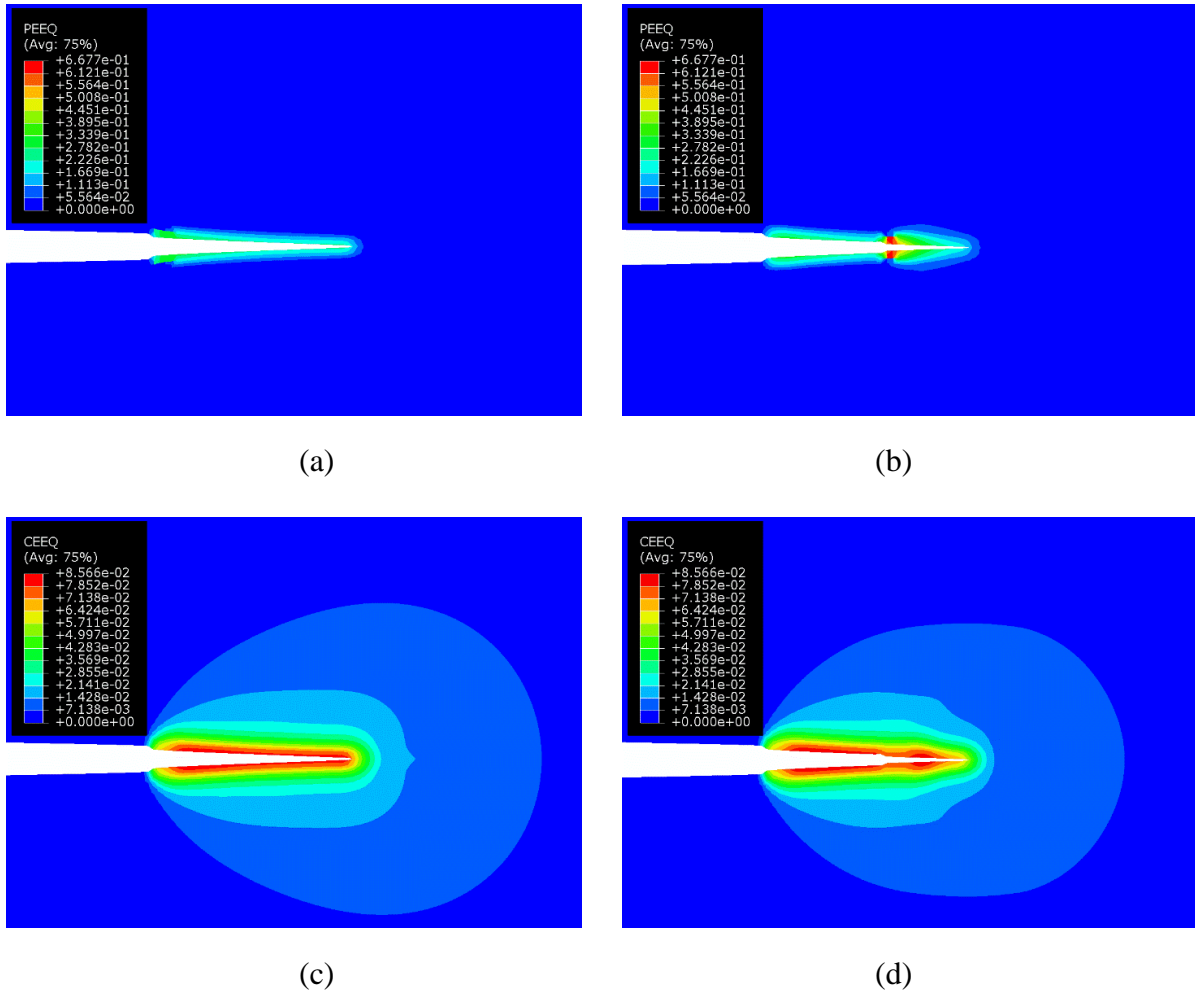


Figure 20. Crack-tip region during CFCG with $t_H = 60$ s in cycle 69 after hold time. Contour plots of equivalent plastic strains for (a) constant amplitude loading and (b) fatigue OL with OLR = 2. Contour plots of equivalent creep strains for (c) constant amplitude loading and (d) fatigue OL with OLR = 2. The OL is applied in cycle 41 (node release 20). The deformation scale factor is 4.

5.4 Single creep-fatigue UL

This section presents the influence of a single creep-fatigue UL applied in a CA CFCG loading waveform. This case is represented schematically in Figure 6d. The CA CFCG waveform has a hold time $t_H = 60$ s. For the creep-fatigue UL, two different ULRs were considered, $ULR = -0.5$ and $ULR = -1$. In the case of $ULR = -0.5$, a single hold time of $t_{UH} = 3600$ s was considered, while in the case of $ULR = -1$, three different hold time in

the UL cycle were considered, i.e., $t_{UH} = 60$ s, $t_{UH} = 600$ s and $t_{UH} = 3600$ s. The evolution of crack-tip opening loads in the case of CA loading and comparisons with values from the UL loading cases are presented in Figure 21. For all the ULR cases, the opening load records a sudden drop that depends on the magnitude of the ULR. The larger the ULR, the larger the initial drop in the opening load. After the initial drop, as the crack advances after the UL is applied, the crack opening loads increase from their minimum value in the UL cycle to eventually join the line that represents the opening loads from CA loading. From this trend, it can be concluded that an UL cycle causes a sudden acceleration in the crack growth rate, which continues for a while until the crack tip advances away from the region influenced by the UL cycle. While the initial decrease in the opening load depends on the magnitude of ULR, the ascending trend in opening loads in the post-UL cycles is the same for all UL and t_{UH} studied.

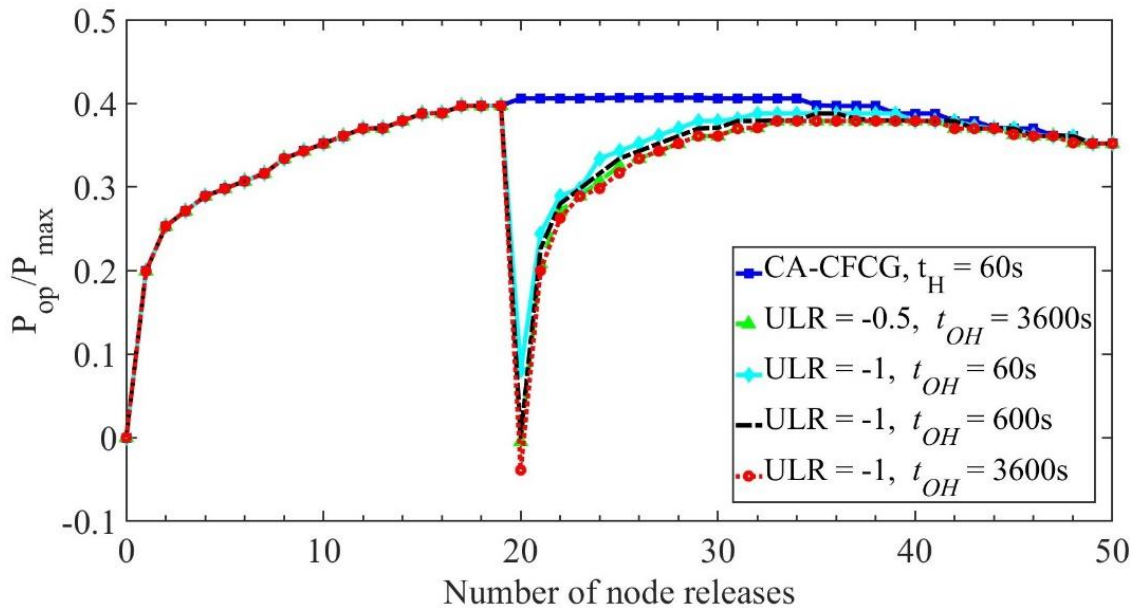


Figure 21. Effects of underload ratio and hold time on crack opening load in CFCG.

CHAPTER 6: CONCLUSIONS AND FUTURE WORK

Crack opening loads during VA loading were simulated in a two-dimensional CT specimen of modified 9Cr-1Mo using the finite element method. Plastic and creep deformations were considered in this study to model the mechanics of crack opening and closing. The conclusions of this study are as follows.

1. An OL inserted in a fatigue or creep-fatigue CA loading waveforms results in a sudden drop in the crack opening load. This is caused by an instantaneous increase in crack-tip opening displacement.
2. After the initial drop caused by the application of the OL, the crack-opening load increase steadily in subsequent cycles.
3. A fatigue OL during FCG and CFCG causes an increase in crack opening loads, as the crack tip is shielded by a thicker plastic wake after the application of OL. Also, the amount of increase in the crack opening compared to values from CA loading is proportional to the OLR.
4. In the case of creep-fatigue OL, the accumulation of inelastic strains ahead of the crack tip leads to a steady increase in plastic wake thickness and greater shielding of the crack tip after the application of the OL cycle. The increase in crack opening load is more significant for larger OLR and longer hold time.
5. The effect of OL in CFCG decreases with the increasing hold time t_H during CA CFCG loading waveforms.
6. The initial decrease in opening load during creep-fatigue UL in CFCG depends on the magnitude of ULR, however, the effect in the post-UL is the same for all ULR and t_{UH} .
7. During the creep-fatigue loading, plastic wake and crack tip blunting tend to stabilize over time. However, despite this relative stabilization, creep deformation continues to accumulate at the crack tip. As a result, the trend of the crack tip opening loads decreases over time. To better control this creep deformation and ensure that the crack opening loads remain stable throughout the simulation, further research is necessary.

REFERENCES

- [1] Grover PS, Saxena A. Development in creep-fatigue crack growth testing and data analysis. In: ECF-10, structural integrity: experiments, models application, vol. 1; 1994. P. 1-21
- [2] Narasimhachary SB, Saxena A. Crack growth behavior of 9Cr–1Mo (P91) steel under creep–fatigue conditions. *Int J Fatigue* 2013;56:106–13.
<https://doi.org/10.1016/J.IJFATIGUE.2013.07.006>.
- [3] Marcello AL, Angelo RM, Filippo B. A unified approach to simulate the creep-fatigue crack growth in P91 steel at elevated temperature under SSY and SSC conditions, *Eng. Fail. Anal.* 127 (2021) 105569,
<https://doi.org/10.1016/j.engfailanal.2021.105569>.
- [4] Ralph IS, Ali F, Robert RS, Henry OF. *Metal Fatigue in Engineering*, Second. Wiley-Interscience, 2001.
- [5] ASTM E2760: Standard Test Method for Measurement of Fatigue Crack Growth Rates
- [6] Paris PC, Erdogan F. A critical analysis of crack propagation laws. *J. Basic Eng-T ASME* 1963;85:528–33.
- [7] Elber W. Fatigue crack growth under cyclic tension. *Eng Fract Mech* 1970;2(1):37-45. [https://doi.org/10.1016/0013-7944\(70\)90028-7](https://doi.org/10.1016/0013-7944(70)90028-7)
- [8] Granacher J, Klenk A, Tramer M, Schellenberg G, Mueller F, Ewald J. Creep fatigue crack behavior of two power plant steels. *Int J Press Vessel Pip* 2001;78:909–20.
[https://doi.org/10.1016/S0308-0161\(01\)00106-5](https://doi.org/10.1016/S0308-0161(01)00106-5).
- [9] Evans WJ, Jones JP, Williams S. The interactions between fatigue, creep and environmental damage in Ti 6246 and Udimet 720Li. *Int J Fatigue* 2005;27:1473–84.
<https://doi.org/10.1016/J.IJFATIGUE.2005.06.029>

- [10] Yoon KB, Saxena A, Liaw PK. Characterization of creep-fatigue crack growth behavior under trapezoidal waveshape using Ct-parameter. *Int J Fatigue* 1994;16:235. [https://doi.org/10.1016/0142-1123\(94\)90089-2](https://doi.org/10.1016/0142-1123(94)90089-2)
- [11] Yang H, Bao R, Zhang J, Peng L, Fei B. Creep-fatigue crack growth behaviour of a nickel-based powder metallurgy superalloy under high temperature. *Eng Fail Anal* 2011;18:1058–66. <https://doi.org/10.1016/J.ENGFAILANAL.2010.12.025>.
- [12] Sehitoglu H, Sun W. The significance of crack closure under high temperature fatigue crack growth with hold periods. *Eng Fract Mech* 1989;33(3):371–88.
- [13] Ramirez J, Potirniche GP, Shaber N, Taylor M, Pugsek H, Stephens R, Charit I. The influence of plasticity-induced crack closure on creep-fatigue crack growth in two heat-resistant steels. *Int. J. Fatigue* 2019;125: 291–298, <https://doi.org/10.1016/j.ijfatigue.2019.04.007>
- [14] Potirniche GP. A closure model for predicting crack growth under creep-fatigue loading. *Int J Fatigue* 2019;125:58-71. <https://doi.org/10.1016/j.ijfatigue.2019.03.029>
- [15] Piard A, Gamby D, Carbou C, Mendez J. A numerical simulation of creep-fatigue crack growth in nickel-base superalloys. *Eng Fract Mech* 2004;71:2299–317. <https://doi.org/10.1016/J.ENGFRACMECH.2004.02.002>.
- [16] Hall DE, Hamilton BC, McDowell DL, Saxena A. Creep crack growth behavior of aluminum alloy 2519: part II—numerical analysis. *Elev Temp Eff fatigue Fract ASTM Int* 1997.
- [17] Ghonem H, Nicholas T, Pineau A. Elevated temperature fatigue crack growth in alloy 718—Part II: effects of environmental and material variables. *Fatigue Fract Eng Mater Struct* 2018;16:577–90. <https://doi.org/10.1111/j.1460-2695.1993.tb00103.x>.
- [18] Espinosa AAA, Fellows NA, Durodola JF, Fellows LJ. Determination of crack growth for 6082-T6 aluminium subjected to periodic single and block overloads and underloads using a two-dimensional finite element model, *Int. J. Fatigue* 105 (2007) 244–261, <https://doi.org/10.1016/j.ijfatigue.2017.08.018>.

- [19] Borrego LP, Ferreira JM, da Cruz JMP, Costa JM. Evaluation of overload effects on fatigue crack growth and closure, *Eng Fract Mech* 70 (2003) 1379–1397.
- [20] Ding Z, Wang X, Gao Z, Bao S. An experimental investigation and prediction of fatigue crack growth under overload/underload in Q345R steel, *Int. J. Fatigue* 98 (2017) 155–166, <https://doi.org/10.1016/j.ijfatigue.2017.01.024>.
- [21] Liang H, Zhan R, Wang DP, Deng CY, Guo BC, Xu XH. Fatigue crack growth under overload/underload indifferent strength structural steel. *J Constr Steel Res.*2022;192:107213.18
- [22] Gong H, Lu YC, Yang FP, Chen T. Experimental study on fatigue crack growth of QSTE420TM steel with a single dwell-overload and a combined prediction model, *J. Constr. Steel Res.* 182 (2021), 106676.
- [23] Saarimäki J, Moverare J, Eriksson R, Johansson S. Influence of overloads on dwell time fatigue crack growth in Inconel 718, *Mater. Sci. Eng.: A* 612 (2014) 398–405, <https://doi.org/10.1016/j.msea.2014.06.068>.
- [24] Pribe JD, Ostergaard HE, Siegmund T, Kruzic JJ. Transient creep-fatigue crack growth in creep-brittle materials: application to Alloy 718. *Fatigue & Fracture of Engineering Materials & Structures*; 2022. <https://doi.org/10.1111/ffe.13788>
- [25] Daniewicz SR, Collins JA, Houser DR. An elastic-plastic analytical model for predicting fatigue crack growth in arbitrary edge-cracked two-dimensional geometries with residual stress. *Int J Fatigue* 1994;16:123–3. [https://doi.org/10.1016/0142-1123\(94\)90102-3](https://doi.org/10.1016/0142-1123(94)90102-3).
- [26] Solanki K, Daniewicz S, Newman J. Finite element modeling of plasticity-induced crack closure with emphasis on geometry and mesh refinement effects. *Eng Fract Mech* 2003;70:1475–89. [https://doi.org/10.1016/S0013-7944\(02\)00168-6](https://doi.org/10.1016/S0013-7944(02)00168-6).
- [27] Dougherty JD, Padovan J, Srivatsan TS. Fatigue crack propagation and closure behavior of modified 1070 steel: Finite element study. *Eng Fract Mech* 1997;56:189–212. [https://doi.org/10.1016/S0013-7944\(96\)00104-X](https://doi.org/10.1016/S0013-7944(96)00104-X).

- [28] de Matos PFP, Nowell D. Numerical simulation of plasticity-induced fatigue crack closure with emphasis on the crack growth scheme: 2D and 3D analyses. *Eng Fract Mech* 2008;75:2087–114. <https://doi.org/10.1016/J.ENGFRACTMECH.2007.10.017>.
- [29] ABAQUS Analysis User's Guide, 2022.

APPENDIX

This appendix presents the input file for finite element simulation of crack growth under CA CFCG with $t_H = 60$ s.

*Heading

** Job name: CFCG_60sH Model name: Model-1

** Generated by: Abaqus/CAE 2022

*Preprint, echo=NO, model=NO, history=NO, contact=NO

**

** PARTS

**

*Part, name=Part-1

*Node

1,	12.5,	3.
2,	0.,	3.
3,	0.,	0.
4,	12.5,	0.
5,	25.,	3.

.....

.....

.....

11126,	26.1865654,	0.
11127,	27.3731289,	1.5
11128,	26.1865654,	1.5
11129,	12.5,	20.
11130,	12.5,	20.

*Element, type=CPS4R

1, 1, 25, 195, 42

2, 25, 26, 196, 195
 3, 26, 27, 197, 196
 4, 27, 28, 198, 197
 5, 28, 29, 199, 198

 10967, 11127, 11118, 11116, 11128
 10968, 11126, 11128, 868, 875
 10969, 11128, 11116, 5, 868
 10970, 11118, 11127, 10790, 10791
 10971, 11127, 11125, 10789, 10792
 *Element, type=CPS3
 10493, 10782, 10761, 10759
 10621, 10863, 10805, 10819
 10633, 813, 10881, 10882
 10972, 11127, 10792, 10790
 *Node
 11131, 32.5, 0., 0.
 *Nset, nset=Part-1-RefPt_, internal
 11131,
 *Nset, nset=Set-259, generate
 1, 11128, 1
 *Elset, elset=Set-259, generate
 1, 10972, 1
 *Elset, elset=AllElements, generate
 1, 10972, 1
 *Nset, nset=AllNodes, generate
 1, 11128, 1
 *Elset, elset=_CT_surface_S1, internal, generate

7999, 8038, 1

*Elset, elset=_CT_surface_S2, internal

10593, 10618, 10624, 10971

*Elset, elset=_CT_surface_S3, internal

10, 11, 12, 13, 14, 15, 16, 17, 18, 722, 723, 724, 725, 726, 727, 728

729, 730, 731, 732, 733, 734, 735, 736

*Elset, elset=_CT_surface_S4, internal

781, 783, 785, 787, 789, 791, 793, 795, 797, 799, 859, 919, 979, 1039,
1099, 1159

1219, 1279, 1339, 1399, 1459, 1519, 1579, 1639, 1699, 1759, 1819, 1879, 1939,
1999, 2059, 2119

2179, 2239, 2299, 2359, 2419, 2479, 2539, 2599, 2659, 2719, 2779, 2839, 2899,
2959, 3019, 3079

3139, 3199, 3259, 3319, 3379, 3439, 3499, 3559, 3619, 3679, 3739, 3799, 3859,
3919, 3979, 4039

4099, 4159, 4219, 4279, 4339, 4399, 4459, 4519, 4579, 4639, 4699, 4759, 4819,
4879, 4939, 4999

5059, 5119, 5179, 5239, 5299, 5359, 5419, 5479, 5539, 5599, 5659, 5719, 5779,
5839, 5899, 5959

6019, 6079, 6139, 6199, 6259, 6319, 6379, 6439, 6499, 6559, 6619, 6679, 6739,
6799, 6859, 6919

6979, 7039, 7099, 7159, 7219, 7279, 7339, 7399, 7459, 7519, 7579, 7639, 7699,
7759, 7819, 7879

7939, 10399, 10459, 10511, 10631, 10966, 10968

*Surface, type=ELEMENT, name=CT_surface

_CT_surface_S1, S1

_CT_surface_S2, S2

_CT_surface_S4, S4

_CT_surface_S3, S3

** Section: Section-1

*Solid Section, elset=Set-259, material=P91_625C

12.5

*End Part

```
**  
  
*Part, name=Wire  
*End Part  
**  
**  
** ASSEMBLY  
**  
*Assembly, name=Assembly  
**  
*Instance, name=Part-1-1, part=Part-1  
*End Instance  
**  
*Instance, name=Wire-1, part=Wire  
    21.25,    0.,    0.  
*Node  
    1,   -28.75,    0.,    0.  
*Nset, nset=Wire-1-RefPt_, internal  
1,  
*Surface, type=SEGMENTS, name=WireSurface  
START,   -28.75,    0.  
LINE,    41.25,    0.  
*End Instance  
**  
*Node  
    1,    32.75,    0.,    0.  
*Node  
    2,    33.,    0.,    0.  
*Node  
    3,    33.25,    0.,    0.  
*Node
```

```

    4,    33.5,    0.,    0.
*Node
    5,    33.75,    0.,    0.
*Node
    6,    34.,    0.,    0.
*Node
    7,    34.25,    0.,    0.
*Node
    8,    34.5,    0.,    0.
*Node
    9,    34.75,    0.,    0.
*Nset, nset=LP, instance=Part-1-1
11130,
*Nset, nset=MPC_points, instance=Part-1-1
  8, 11, 12, 16, 66, 67, 68, 69, 70, 71, 72, 73, 74, 75, 76, 77
 78, 79, 102, 103, 104, 105, 106, 107, 108, 141, 142, 143, 144, 145, 146, 147
*Nset, nset=RP, instance=Wire-1
 1,
*Nset, nset=Y1, instance=Part-1-1
 794, 795, 796, 797, 798, 799, 800, 801, 803, 804, 805, 806, 822, 825, 826,
827
 990, 993, 1015, 1021, 1032, 1033, 1233, 1234, 1235, 1236, 1237, 1238, 1239,
1240, 1241, 1242
 1243, 1244, 1245, 1246, 1247, 1248, 1249, 1250, 1251, 1252, 1253, 1254, 1255,
1256, 1257, 1258
 1259, 1260, 1261, 1262, 1263, 1264, 1265, 1266, 1267, 1268, 1269, 1270, 1271,
1272, 1273, 1274
 1275, 1276, 1277, 1278, 1279, 1280, 1281, 1282, 1283, 1284, 1285, 1286, 1287,
1288, 1289, 1290
 1291, 1292, 1293, 1294, 1295, 1296, 1297, 1298, 1299, 1300, 1301, 1302, 1303,
1304, 1305, 1306

```

1307, 1308, 1309, 1310, 1311, 1312, 1313, 1314, 1315, 1316, 1317, 1318, 1319,
1320, 1321, 1322

1323, 1324, 1325, 1326, 1327, 1328, 1329, 1330, 1331, 1332, 1333, 1334, 1335,
1336, 1337, 1338

1339, 1340, 1341, 1342, 1343, 1344, 1345, 1346, 10814, 10861, 10880

*Nset, nset=Y2, instance=Part-1-1

794, 795, 796, 797, 798, 799, 800, 801, 803, 804, 805, 806, 822, 825, 826,
827

990, 993, 1015, 1021, 1032, 1033, 1234, 1235, 1236, 1237, 1238, 1239, 1240,
1241, 1242, 1243

1244, 1245, 1246, 1247, 1248, 1249, 1250, 1251, 1252, 1253, 1254, 1255, 1256,
1257, 1258, 1259

1260, 1261, 1262, 1263, 1264, 1265, 1266, 1267, 1268, 1269, 1270, 1271, 1272,
1273, 1274, 1275

1276, 1277, 1278, 1279, 1280, 1281, 1282, 1283, 1284, 1285, 1286, 1287, 1288,
1289, 1290, 1291

1292, 1293, 1294, 1295, 1296, 1297, 1298, 1299, 1300, 1301, 1302, 1303, 1304,
1305, 1306, 1307

1308, 1309, 1310, 1311, 1312, 1313, 1314, 1315, 1316, 1317, 1318, 1319, 1320,
1321, 1322, 1323

1324, 1325, 1326, 1327, 1328, 1329, 1330, 1331, 1332, 1333, 1334, 1335, 1336,
1337, 1338, 1339

1340, 1341, 1342, 1343, 1344, 1345, 1346, 10814, 10861, 10880

*Nset, nset=Y3, instance=Part-1-1

794, 795, 796, 797, 798, 799, 800, 801, 803, 804, 805, 806, 822, 825, 826,
827

990, 993, 1015, 1021, 1032, 1033, 1235, 1236, 1237, 1238, 1239, 1240, 1241,
1242, 1243, 1244

1245, 1246, 1247, 1248, 1249, 1250, 1251, 1252, 1253, 1254, 1255, 1256, 1257,
1258, 1259, 1260

1261, 1262, 1263, 1264, 1265, 1266, 1267, 1268, 1269, 1270, 1271, 1272, 1273,
1274, 1275, 1276

1277, 1278, 1279, 1280, 1281, 1282, 1283, 1284, 1285, 1286, 1287, 1288, 1289,
1290, 1291, 1292

1293, 1294, 1295, 1296, 1297, 1298, 1299, 1300, 1301, 1302, 1303, 1304, 1305,
1306, 1307, 1308

1309, 1310, 1311, 1312, 1313, 1314, 1315, 1316, 1317, 1318, 1319, 1320, 1321,
1322, 1323, 1324

1325, 1326, 1327, 1328, 1329, 1330, 1331, 1332, 1333, 1334, 1335, 1336, 1337,
1338, 1339, 1340

1341, 1342, 1343, 1344, 1345, 1346, 10814, 10861, 10880

*Nset, nset=Y4, instance=Part-1-1

794, 795, 796, 797, 798, 799, 800, 801, 803, 804, 805, 806, 822, 825, 826,
827

990, 993, 1015, 1021, 1032, 1033, 1236, 1237, 1238, 1239, 1240, 1241, 1242,
1243, 1244, 1245

1246, 1247, 1248, 1249, 1250, 1251, 1252, 1253, 1254, 1255, 1256, 1257, 1258,
1259, 1260, 1261

1262, 1263, 1264, 1265, 1266, 1267, 1268, 1269, 1270, 1271, 1272, 1273, 1274,
1275, 1276, 1277

1278, 1279, 1280, 1281, 1282, 1283, 1284, 1285, 1286, 1287, 1288, 1289, 1290,
1291, 1292, 1293

1294, 1295, 1296, 1297, 1298, 1299, 1300, 1301, 1302, 1303, 1304, 1305, 1306,
1307, 1308, 1309

1310, 1311, 1312, 1313, 1314, 1315, 1316, 1317, 1318, 1319, 1320, 1321, 1322,
1323, 1324, 1325

1326, 1327, 1328, 1329, 1330, 1331, 1332, 1333, 1334, 1335, 1336, 1337, 1338,
1339, 1340, 1341

1342, 1343, 1344, 1345, 1346, 10814, 10861, 10880

*Nset, nset=Y5, instance=Part-1-1

794, 795, 796, 797, 798, 799, 800, 801, 803, 804, 805, 806, 822, 825, 826,
827

990, 993, 1015, 1021, 1032, 1033, 1237, 1238, 1239, 1240, 1241, 1242, 1243,
1244, 1245, 1246

1247, 1248, 1249, 1250, 1251, 1252, 1253, 1254, 1255, 1256, 1257, 1258, 1259,
1260, 1261, 1262

1263, 1264, 1265, 1266, 1267, 1268, 1269, 1270, 1271, 1272, 1273, 1274, 1275,
1276, 1277, 1278

1279, 1280, 1281, 1282, 1283, 1284, 1285, 1286, 1287, 1288, 1289, 1290, 1291,
1292, 1293, 1294

1295, 1296, 1297, 1298, 1299, 1300, 1301, 1302, 1303, 1304, 1305, 1306, 1307,
1308, 1309, 1310

1311, 1312, 1313, 1314, 1315, 1316, 1317, 1318, 1319, 1320, 1321, 1322, 1323,
1324, 1325, 1326

1327, 1328, 1329, 1330, 1331, 1332, 1333, 1334, 1335, 1336, 1337, 1338, 1339,
1340, 1341, 1342

1343, 1344, 1345, 1346, 10814, 10861, 10880

.....

.....

.....

*Nset, nset=Y51, instance=Part-1-1

794, 795, 796, 797, 798, 799, 800, 801, 803, 804, 805, 806, 822, 825, 826,
827

990, 993, 1015, 1021, 1032, 1033, 1283, 1284, 1285, 1286, 1287, 1288, 1289,
1290, 1291, 1292

1293, 1294, 1295, 1296, 1297, 1298, 1299, 1300, 1301, 1302, 1303, 1304, 1305,
1306, 1307, 1308

1309, 1310, 1311, 1312, 1313, 1314, 1315, 1316, 1317, 1318, 1319, 1320, 1321,
1322, 1323, 1324

1325, 1326, 1327, 1328, 1329, 1330, 1331, 1332, 1333, 1334, 1335, 1336, 1337,
1338, 1339, 1340

1341, 1342, 1343, 1344, 1345, 1346, 10814, 10861, 10880

*Nset, nset=Y52, instance=Part-1-1

794, 795, 796, 797, 798, 799, 800, 801, 803, 804, 805, 806, 822, 825, 826,
827

990, 993, 1015, 1021, 1032, 1033, 1284, 1285, 1286, 1287, 1288, 1289, 1290,
1291, 1292, 1293

1294, 1295, 1296, 1297, 1298, 1299, 1300, 1301, 1302, 1303, 1304, 1305, 1306,
1307, 1308, 1309

1310, 1311, 1312, 1313, 1314, 1315, 1316, 1317, 1318, 1319, 1320, 1321, 1322,
1323, 1324, 1325

1326, 1327, 1328, 1329, 1330, 1331, 1332, 1333, 1334, 1335, 1336, 1337, 1338,
1339, 1340, 1341

1342, 1343, 1344, 1345, 1346, 10814, 10861, 10880

*Nset, nset=YNodes, instance=Part-1-1

794, 795, 796, 797, 798, 799, 800, 801, 803, 804, 805, 806, 822, 825, 826,
827

955, 990, 993, 1015, 1021, 1032, 1033, 1233, 1234, 1235, 1236, 1237, 1238,
1239, 1240, 1241

1242, 1243, 1244, 1245, 1246, 1247, 1248, 1249, 1250, 1251, 1252, 1253, 1254,
1255, 1256, 1257

1258, 1259, 1260, 1261, 1262, 1263, 1264, 1265, 1266, 1267, 1268, 1269, 1270,
1271, 1272, 1273

1274, 1275, 1276, 1277, 1278, 1279, 1280, 1281, 1282, 1283, 1284, 1285, 1286,
1287, 1288, 1289

1290, 1291, 1292, 1293, 1294, 1295, 1296, 1297, 1298, 1299, 1300, 1301, 1302,
1303, 1304, 1305

1306, 1307, 1308, 1309, 1310, 1311, 1312, 1313, 1314, 1315, 1316, 1317, 1318,
1319, 1320, 1321

1322, 1323, 1324, 1325, 1326, 1327, 1328, 1329, 1330, 1331, 1332, 1333, 1334,
1335, 1336, 1337

1338, 1339, 1340, 1341, 1342, 1343, 1344, 1345, 1346, 10814, 10861, 10880

*Nset, nset=_PickedSet18, internal, instance=Wire-1

1,

*Surface, type=NODE, name=MPC_points_CNS_, internal

MPC_points, 1.

** Constraint: MPC-Constraint-1

*MPC

LINK, MPC_points, LP

** Constraint: RigidBody

*Rigid Body, ref node=_PickedSet18, analytical surface=Wire-1.WireSurface

*End Assembly

**

** MATERIALS

**

*Material, name=P91_625C

```

*Creep
9.53e-21, 8.24, 0.
*Elastic
125000., 0.3
*Plastic
334.4, 0.
**
** INTERACTION PROPERTIES
**
*Surface Interaction, name=IntProp-1
1.,
*Surface Behavior, augmented Lagrange
**
** BOUNDARY CONDITIONS
**
** Name: BC-1 Type: Symmetry/Antisymmetry/Encastre
*Boundary
RP, ENCASTRE
** Name: BC-2 Type: Displacement/Rotation
*Boundary
LP, 1, 1
** Name: BC-3 Type: Displacement/Rotation
*Boundary
YNodes, 2, 2
**
** INTERACTIONS
**
** Interaction: Int-1
*Contact Pair, interaction=IntProp-1
Part-1-1.CT_surface, Wire-1.WireSurface

```

```
** -----  
**  
** STEP: L1  
**  
*Step, name=L1, nlgeom=NO  
*Static, direct  
0.01, 1.,  
**  
** LOADS  
**  
** Name: Load-1  Type: Concentrated force  
*Cload, op=NEW  
LP, 2, 8100.  
**  
** OUTPUT REQUESTS  
**  
*Restart, write, frequency=0  
**  
** FIELD OUTPUT: F-Output-1  
**  
*Output, field, variable=PRESELECT  
**  
** HISTORY OUTPUT: H-Output-1  
**  
*Output, history, variable=PRESELECT  
*End Step  
** -----  
**  
** STEP: H1  
**
```

```
*Step, name=H1, nlgeom=NO, inc=50000
*Visco, cetol=1e-05
1e-07, 0.0166667, 1e-14, 0.0166667
**
** LOADS
**
** Name: Load-1  Type: Concentrated force
*Cloud, op=NEW
LP, 2, 8100.
**
** OUTPUT REQUESTS
**
*Restart, write, frequency=0
**
** FIELD OUTPUT: F-Output-2
**
*Output, field, variable=PRESELECT
**
** HISTORY OUTPUT: H-Output-2
**
*Output, history, variable=PRESELECT
*End Step
** -----
**
** STEP: U1
**
*Step, name=U1, nlgeom=NO
*Static, direct
0.01, 1.,
**
```

**** LOADS************ Name: Load-1 Type: Concentrated force*****Cloud, op=NEW****** Name: Load-2 Type: Concentrated force*****Cloud, op=NEW****LP, 2, 810.************ OUTPUT REQUESTS***********Restart, write, frequency=0************ FIELD OUTPUT: F-Output-3***********Output, field, variable=PRESELECT************ HISTORY OUTPUT: H-Output-3***********Output, history, variable=PRESELECT*****End Step****** -----************ STEP: L1B***********Step, name=L1B, nlgeom=NO*****Static, direct****0.01, 1.,************ LOADS********

** Name: Load-2 Type: Concentrated force

*Cload, op=NEW

** Name: Load-3 Type: Concentrated force

*Cload, op=NEW

LP, 2, 8100.

**

** OUTPUT REQUESTS

**

*Restart, write, frequency=0

**

** FIELD OUTPUT: F-Output-4

**

*Output, field, variable=PRESELECT

**

** HISTORY OUTPUT: H-Output-4

**

*Output, history, variable=PRESELECT

*End Step

** -----

**

** STEP: H1B

**

*Step, name=H1B, nlgeom=NO, inc=50000

*Visco, cetol=1e-05

1e-07, 0.0166667, 1e-14, 0.0166667

**

** LOADS

**

** Name: Load-3 Type: Concentrated force

*Cload, op=NEW

LP, 2, 8100.

**

** OUTPUT REQUESTS

**

*Restart, write, frequency=0

**

** FIELD OUTPUT: F-Output-5

**

*Output, field, variable=PRESELECT

**

** HISTORY OUTPUT: H-Output-5

**

*Output, history, variable=PRESELECT

*End Step

** -----

**

** STEP: U1B

**

*Step, name=U1B, nlgeom=NO

*Static, direct

0.01, 1.,

**

** LOADS

**

** Name: Load-3 Type: Concentrated force

*Cload, op=NEW

** Name: Load-4 Type: Concentrated force

*Cload, op=NEW

LP, 2, 810.

**

**** OUTPUT REQUESTS***********Restart, write, frequency=0************ FIELD OUTPUT: F-Output-6***********Output, field, variable=PRESELECT************ HISTORY OUTPUT: H-Output-6***********Output, history, variable=PRESELECT*****End Step****** -----************ STEP: L2***********Step, name=L2, nlgeom=NO*****Static, direct****0.01, 1.,************ BOUNDARY CONDITIONS************ Name: BC-1 Type: Symmetry/Antisymmetry/Encastre*****Boundary, op=NEW****** Name: BC-2 Type: Displacement/Rotation*****Boundary, op=NEW****** Name: BC-3 Type: Displacement/Rotation*****Boundary, op=NEW****** Name: BC-4 Type: Symmetry/Antisymmetry/Encastre*****Boundary, op=NEW**

RP, ENCASTRE

** Name: BC-5 Type: Displacement/Rotation

*Boundary, op=NEW

LP, 1, 1

** Name: BC-6 Type: Displacement/Rotation

*Boundary, op=NEW

Y1, 2, 2

**

** LOADS

**

** Name: Load-4 Type: Concentrated force

*Cload, op=NEW

** Name: Load-5 Type: Concentrated force

*Cload, op=NEW

LP, 2, 8100.

**

** OUTPUT REQUESTS

**

*Restart, write, frequency=0

**

** FIELD OUTPUT: F-Output-7

**

*Output, field, variable=PRESELECT

**

** HISTORY OUTPUT: H-Output-7

**

*Output, history, variable=PRESELECT

*End Step

** -----

**

```
** STEP: H2
**
**
*Step, name=H2, nlgeom=NO, inc=50000
*Visco, cetol=1e-05
1e-07, 0.0166667, 1e-14, 0.0166667
**
** LOADS
**
** Name: Load-5  Type: Concentrated force
*Clod, op=NEW
LP, 2, 8100.
**
** OUTPUT REQUESTS
**
**
*Restart, write, frequency=0
**
** FIELD OUTPUT: F-Output-8
**
**
*Output, field, variable=PRESELECT
**
** HISTORY OUTPUT: H-Output-8
**
**
*Output, history, variable=PRESELECT
*End Step
** -----
**
** STEP: U2
**
**
*Step, name=U2, nlgeom=NO
*Static, direct
```

0.01, 1.,
**
** LOADS
**
** Name: Load-5 Type: Concentrated force
*Cload, op=NEW
** Name: Load-6 Type: Concentrated force
*Cload, op=NEW
LP, 2, 810.
**
** OUTPUT REQUESTS
**
*Restart, write, frequency=0
**
** FIELD OUTPUT: F-Output-9
**
*Output, field, variable=PRESELECT
**
** HISTORY OUTPUT: H-Output-9
**
*Output, history, variable=PRESELECT
*End Step
** -----
**
** STEP: L2B
**
*Step, name=L2B, nlgeom=NO
*Static, direct
0.01, 1.,
**

**** LOADS************ Name: Load-6 Type: Concentrated force*****Cloud, op=NEW****** Name: Load-7 Type: Concentrated force*****Cloud, op=NEW****LP, 2, 8100.************ OUTPUT REQUESTS***********Restart, write, frequency=0************ FIELD OUTPUT: F-Output-10***********Output, field, variable=PRESELECT************ HISTORY OUTPUT: H-Output-10***********Output, history, variable=PRESELECT*****End Step****** -----************ STEP: H2B***********Step, name=H2B, nlgeom=NO, inc=50000*****Visco, cetol=1e-05****1e-07, 0.0166667, 1e-14, 0.0166667************ LOADS********

** Name: Load-7 Type: Concentrated force

*Cload, op=NEW

LP, 2, 8100.

**

** OUTPUT REQUESTS

**

*Restart, write, frequency=0

**

** FIELD OUTPUT: F-Output-11

**

*Output, field, variable=PRESELECT

**

** HISTORY OUTPUT: H-Output-11

**

*Output, history, variable=PRESELECT

*End Step

** -----

**

** STEP: U2B

**

*Step, name=U2B, nlgeom=NO

*Static, direct

0.01, 1.,

**

** LOADS

**

** Name: Load-7 Type: Concentrated force

*Cload, op=NEW

** Name: Load-8 Type: Concentrated force

*Cload, op=NEW

LP, 2, 810.

**

** OUTPUT REQUESTS

**

*Restart, write, frequency=0

**

** FIELD OUTPUT: F-Output-12

**

*Output, field, variable=PRESELECT

**

** HISTORY OUTPUT: H-Output-12

**

*Output, history, variable=PRESELECT

*End Step

.....

.....

.....

** -----

**

** STEP: L49

**

*Step, name=L49, nlgeom=NO, inc=150

*Static

0.01, 1., 1e-05, 0.01

**

** BOUNDARY CONDITIONS

**

** Name: BC-142 Type: Displacement/Rotation

*Boundary, op=NEW


```
** Name: BC-143 Type: Displacement/Rotation
*Boundary, op=NEW
** Name: BC-144 Type: Symmetry/Antisymmetry/Encastre
*Boundary, op=NEW
** Name: BC-145 Type: Symmetry/Antisymmetry/Encastre
*Boundary, op=NEW
RP, ENCASTRE
** Name: BC-146 Type: Displacement/Rotation
*Boundary, op=NEW
LP, 1, 1
** Name: BC-147 Type: Displacement/Rotation
*Boundary, op=NEW
Y48, 2, 2
**
** LOADS
**
** Name: Load-193 Type: Concentrated force
*Clod, op=NEW
** Name: Load-194 Type: Concentrated force
*Clod, op=NEW
LP, 2, 8100.
**
** OUTPUT REQUESTS
**
*Restart, write, frequency=0
**
** FIELD OUTPUT: F-Output-183, F-Output-289
**
*Output, field, variable=PRESELECT
**
```

** HISTORY OUTPUT: H-Output-183, H-Output-289

**

*Output, history, variable=PRESELECT

*End Step

** -----

**

** STEP: H49

**

*Step, name=H49, nlgeom=NO, inc=50000

*Visco, cetol=1e-05

1e-07, 0.0166667, 1e-14, 0.0166667

**

** LOADS

**

** Name: Load-194 Type: Concentrated force

*Cload, op=NEW

LP, 2, 8100.

**

** OUTPUT REQUESTS

**

*Restart, write, frequency=0

**

** FIELD OUTPUT: F-Output-183, F-Output-290

**

*Output, field, variable=PRESELECT

**

** HISTORY OUTPUT: H-Output-183, H-Output-290

**

*Output, history, variable=PRESELECT

*End Step

```
** -----  
**  
** STEP: U49  
**  
*Step, name=U49, nlgeom=NO, inc=150  
*Static  
0.01, 1., 1e-05, 0.01  
**  
** LOADS  
**  
** Name: Load-194 Type: Concentrated force  
*Cload, op=NEW  
** Name: Load-195 Type: Concentrated force  
*Cload, op=NEW  
LP, 2, 810.  
**  
** OUTPUT REQUESTS  
**  
*Restart, write, frequency=0  
**  
** FIELD OUTPUT: F-Output-183, F-Output-291  
**  
*Output, field, variable=PRESELECT  
**  
** HISTORY OUTPUT: H-Output-183, H-Output-291  
**  
*Output, history, variable=PRESELECT  
*End Step  
** -----  
**
```

```
** STEP: L49B
**
*Step, name=L49B, nlgeom=NO, inc=150
*Static
0.01, 1., 1e-05, 0.01
**
** LOADS
**
** Name: Load-195  Type: Concentrated force
*Clod, op=NEW
** Name: Load-196  Type: Concentrated force
*Clod, op=NEW
LP, 2, 8100.
**
** OUTPUT REQUESTS
**
*Restart, write, frequency=0
**
** FIELD OUTPUT: F-Output-183, F-Output-292
**
*Output, field, variable=PRESELECT
**
** HISTORY OUTPUT: H-Output-183, H-Output-292
**
*Output, history, variable=PRESELECT
*End Step
** -----
**
** STEP: H49B
**
```

```
*Step, name=H49B, nlgeom=NO, inc=50000
*Visco, cetol=1e-05
1e-07, 0.0166667, 1e-14, 0.0166667
**
** LOADS
**
** Name: Load-196  Type: Concentrated force
*Cload, op=NEW
LP, 2, 8100.
**
** OUTPUT REQUESTS
**
*Restart, write, frequency=0
**
** FIELD OUTPUT: F-Output-183, F-Output-293
**
*Output, field, variable=PRESELECT
**
** HISTORY OUTPUT: H-Output-183, H-Output-293
**
*Output, history, variable=PRESELECT
*End Step
** -----
**
** STEP: U49B
**
*Step, name=U49B, nlgeom=NO, inc=150
*Static
0.01, 1., 1e-05, 0.01
**
```

**** LOADS************ Name: Load-196 Type: Concentrated force*****Cload, op=NEW****** Name: Load-197 Type: Concentrated force*****Cload, op=NEW****LP, 2, 810.************ OUTPUT REQUESTS***********Restart, write, frequency=0************ FIELD OUTPUT: F-Output-183, F-Output-294***********Output, field, variable=PRESELECT************ HISTORY OUTPUT: H-Output-183, H-Output-294***********Output, history, variable=PRESELECT*****End Step****** -----************ STEP: L50***********Step, name=L50, nlgeom=NO, inc=150*****Static****0.01, 1., 1e-05, 0.01************ BOUNDARY CONDITIONS********

** Name: BC-145 Type: Symmetry/Antisymmetry/Encastre

*Boundary, op=NEW

** Name: BC-146 Type: Displacement/Rotation

*Boundary, op=NEW

** Name: BC-147 Type: Displacement/Rotation

*Boundary, op=NEW

** Name: BC-148 Type: Displacement/Rotation

*Boundary, op=NEW

Y49, 2, 2

** Name: BC-149 Type: Displacement/Rotation

*Boundary, op=NEW

LP, 1, 1

** Name: BC-150 Type: Symmetry/Antisymmetry/Encastre

*Boundary, op=NEW

RP, ENCASTRE

**

** LOADS

**

** Name: Load-197 Type: Concentrated force

*Cload, op=NEW

** Name: Load-198 Type: Concentrated force

*Cload, op=NEW

LP, 2, 8100.

**

** OUTPUT REQUESTS

**

*Restart, write, frequency=0

**

** FIELD OUTPUT: F-Output-183, F-Output-295

**

```
*Output, field, variable=PRESELECT
**
** HISTORY OUTPUT: H-Output-183, H-Output-295
**
*Output, history, variable=PRESELECT
*End Step
** -----
**
** STEP: H50
**
*Step, name=H50, nlgeom=NO, inc=50000
*Visco, cetol=1e-05
1e-07, 0.0166667, 1e-14, 0.0166667
**
** LOADS
**
** Name: Load-198  Type: Concentrated force
*Cloud, op=NEW
LP, 2, 8100.
**
** OUTPUT REQUESTS
**
*Restart, write, frequency=0
**
** FIELD OUTPUT: F-Output-183, F-Output-296
**
*Output, field, variable=PRESELECT
**
** HISTORY OUTPUT: H-Output-183, H-Output-296
**
```



```
*Output, history, variable=PRESELECT
*End Step
** -----
**
** STEP: U50
**
*Step, name=U50, nlgeom=NO, inc=150
*Static
0.01, 1., 1e-05, 0.01
**
** LOADS
**
** Name: Load-198  Type: Concentrated force
*Clod, op=NEW
** Name: Load-199  Type: Concentrated force
*Clod, op=NEW
LP, 2, 810.
**
** OUTPUT REQUESTS
**
*Restart, write, frequency=0
**
** FIELD OUTPUT: F-Output-183, F-Output-297
**
*Output, field, variable=PRESELECT
**
** HISTORY OUTPUT: H-Output-183, H-Output-297
**
*Output, history, variable=PRESELECT
*End Step
```

```
** -----  
**  
** STEP: L50B  
**  
*Step, name=L50B, nlgeom=NO, inc=150  
*Static  
0.01, 1., 1e-05, 0.01  
**  
** LOADS  
**  
** Name: Load-199 Type: Concentrated force  
*Cload, op=NEW  
** Name: Load-200 Type: Concentrated force  
*Cload, op=NEW  
LP, 2, 8100.  
**  
** OUTPUT REQUESTS  
**  
*Restart, write, frequency=0  
**  
** FIELD OUTPUT: F-Output-183, F-Output-298  
**  
*Output, field, variable=PRESELECT  
**  
** HISTORY OUTPUT: H-Output-183, H-Output-298  
**  
*Output, history, variable=PRESELECT  
*End Step  
** -----  
**
```

```
** STEP: H50B
**
*Step, name=H50B, nlgeom=NO, inc=50000
*Visco, cetol=1e-05
1e-07, 0.0166667, 1e-14, 0.0166667
**
** LOADS
**
** Name: Load-200  Type: Concentrated force
*Clod, op=NEW
LP, 2, 8100.
**
** OUTPUT REQUESTS
**
*Restart, write, frequency=0
**
** FIELD OUTPUT: F-Output-183, F-Output-299
**
*Output, field, variable=PRESELECT
**
** HISTORY OUTPUT: H-Output-183, H-Output-299
**
*Output, history, variable=PRESELECT
*End Step
** -----
**
** STEP: U50B
**
*Step, name=U50B, nlgeom=NO, inc=150
*Static
```

0.01, 1., 1e-05, 0.01

**

** LOADS

**

** Name: Load-200 Type: Concentrated force

*Cload, op=NEW

** Name: Load-201 Type: Concentrated force

*Cload, op=NEW

LP, 2, 810.

**

** OUTPUT REQUESTS

**

*Restart, write, frequency=0

**

** FIELD OUTPUT: F-Output-183, F-Output-300

**

*Output, field, variable=PRESELECT

**

** HISTORY OUTPUT: H-Output-183, H-Output-300

**

*Output, history, variable=PRESELECT

*End Step